

Self-consistent solution for the generalized hydrodynamics model of suspension dynamics: Comparison of theory with rheological and optical measurements

Norman J. Wagner

Department of Chemical Engineering, University of Delaware, Newark, Delaware 19716

(Received 20 May 1993)

A self-consistent theory for the dynamics and rheology of suspensions of Brownian colloids is presented completely in terms of physicochemical suspensions properties. The theory uses the Rogers-Young closure [Phys. Rev. A **30**, 999 (1984)] of the Ornstein-Zernike equation for the equilibrium structure and the generalized hydrodynamics theory developed by Hess and Klein [Adv. Phys. **33**, 173 (1983)] for the dynamic properties. Direct hydrodynamic interactions are neglected. Mode-mode coupling is used to close the generalized hydrodynamics equations and provide a self-consistent set of equations for the dynamics. Two closures for the three-particle vertex function, a two-body approximation and convolution, are derived and compared. All accessible linear viscoelastic properties of the suspension are then calculated from the dynamics of the intermediate-scattering function. Numerical solutions are obtained for Yukawa particles through the viscoelastic approximation. Comparisons with dynamic-light-scattering measurements of the cumulants and the intermediate-scattering function of dilute but strongly correlated suspensions demonstrate the accuracy of the self-consistent solution with the two-body approximation for low particle concentrations. Comparisons of the mechanical properties of concentrated, strongly correlated suspensions demonstrate the accuracy of the self-consistent solutions with the convolution approximation. The results are interpreted in terms of the cage-melting model for colloid dynamics.

PACS number(s): 66.20.+d, 82.70.Dd, 05.60.+w, 82.70.Kj

I. INTRODUCTION

One important aim of applying statistical mechanics to describe the dynamics of Brownian suspensions has been to predict the measurable dynamic and rheological properties, such as the dynamic relaxation of density fluctuations and the frequency-dependent shear viscosity, solely in terms of the fundamental interparticle interactions. Understanding the macroscopic ramifications of changing the nature of the microscopic forces acting on the colloidal level is a challenging problem with a rich history and is of obvious technological importance. As with molecular fluids, it is the collective, many-body interactions that provide the wealth of interesting behavior one hopes to explain in terms of the microscopic forces between the individual Brownian particles. The advent of larger computers and the application of methods designed to tackle many-body interactions in statistical mechanics make a direct comparison of predicted and measured dynamics now feasible. Because of the long time and length scales involved in probing macromolecular fluids (versus molecular fluids), there is relatively easy experimental access to both macroscopic and colloidal level properties for comparison with theory. Further, from an engineering, modeling standpoint, it is important to have a fundamental theoretical foundation to judge the applicability of more phenomenological approaches. It is the goal of this paper to provide a self-consistent statistical mechanical description of dense fluid dynamics and rheology valid for colloidal suspensions that connects the

colloidal level interactions to the macroscopic properties and to test the validity of this theory directly against experiments on a model colloidal suspension.

The method for describing the dynamics of Brownian suspensions is based on the mode-coupling closure of a system of generalized hydrodynamic equations [1–10]. It should be noted that a similar approach has had marked success in elucidating the dynamics of *molecular* fluids, in contrast to the *macromolecular* fluids considered here, for over a decade [11–16]. The theory yields a set of self-consistent equations for the collective dynamics of a fluid composed of Brownian particles completely in terms of the static structure of the suspension. Since there are now accurate solutions for the structure of charged, Brownian particles in terms of the intercolloidal potentials [17–19], a direct link between the underlying microscopic forces and the dynamics of Brownian suspensions is possible. In this paper, these two developments are combined and a method for numerically calculating a self-consistent solution for the dynamics, starting only from the basic physicochemical properties of the Brownian particles and the solvent, is derived. Further, the linear viscoelastic rheological properties are derived in terms of the collective dynamics of density relaxations. Thus the viscosity of the suspension in the limit of linear response is also calculated directly from the physicochemical colloidal properties.

Significant comparisons have been made between predictions of the generalized hydrodynamics approach for dilute, weakly interacting polystyrene colloid suspensions [1,10,20], concentrated suspension self-diffusion [21,22],

and for hard-sphere colloidal glasses [16,23–26]. Although mechanical measurements of collective dynamics are quite prevalent in the literature, actual quantitative comparison of theories based on generalized hydrodynamics against rheological measurements on concentrated, fluid systems are absent. As will also be shown here, dynamic-light-scattering (DLS) measurements of collective structure relaxations provide quantitative tests of the detailed predictions of this theory. In the concentrated regime, DLS measurements are difficult for all but a few index matched systems; however, rheological measurements become feasible and provide quantitative tests of the theoretical predictions.

This theory can be contrasted with an alternative, but complementary, approach based on solving a nonequilibrium Smoluchowski equation for an applied shear field [27–36]. The necessary inputs include the equilibrium microstructure, the microscopic interaction forces, and closure relations for many-body distribution functions. By ensemble averaging the microscopic stresses resulting from the interactions between the Brownian particles over this nonequilibrium microstructure, the theory predicts the bulk stresses in the deforming suspension (principally the low shear limiting viscosity). Again, rheological measurements of the low shear limiting viscosity provide quantitative tests. Further, static light and neutron scattering measurements of the nonequilibrium microstructure provide quantitative tests of the predictions for the steady nonequilibrium microstructure [30,37–42]. In comparison, one advantage of using the generalized hydrodynamics approach employed here is the formulation of a self-consistent set of equations for the full dynamics of the suspension through the mode-mode-coupling ansatz. Further, generalized hydrodynamics yields the full time dependence of all measurable quantities, such as densities and fluxes, as part of the self-consistent solution.

In what follows, the theoretical approach is reviewed and solutions for a model system of charged, Brownian particles are presented. The effect of polydispersity on suspension properties is included in the cumulant and equilibrium structure calculations, along with an examination of the primary electroviscous effect. The generalized hydrodynamics equations are defined and the mode-mode-coupling closure invoked. Two different closures for the resultant three-body vertex functions are derived and compared. A tractable numerical solution of the self-consistent equations is obtained through the use of the viscoelastic approximation. This also enables asymptotic examination of the strong-coupling limit and the glass transition. Numerical calculation of the self-consistent equations and comparison to DLS and rheological experiments for a well-characterized model system are made to test the validity of the theory. As will be demonstrated by quantitative comparison with experiment, the theory captures the basic physics of concentrated suspensions, including the divergence of the Maxwell relaxation time associated with the shear viscosity as an ideal-glass transition is approached. Finally, a physical picture of the generalized hydrodynamic theory with mode-mode cou-

pling is presented through the cage-melting model and a possible criterion for the ideal-glass transition discussed.

II. EQUILIBRIUM SUSPENSION PROPERTIES

A. Microstructure

To define the model systems of interest in this study and to connect the physicochemical properties of the suspension to the equilibrium structure, an integral equation approach is defined as follows. The equilibrium microstructure of a suspension is characterized by the radial distribution function $g(r)$, which is proportional to the probability of finding a particle at the relative distance r from the origin given that a particle is centered at this origin. This function can be calculated from the Ornstein-Zernike equation (OZ) [17]

$$h(r_{12}) = g(r_{12}) - 1 = c_d(r_{12}) + C \int c_d(r_{13})h(r_{23})d\mathbf{x}_3, \quad (1)$$

where $c_d(r)$ is the direct correlation function and C is the number density of the colloidal particles. A closure relation is needed to connect $h(r)$ and $c_d(r)$ with the interaction potential. The Rogers-Young scheme (RY) [18], which mixes the well known Percus-Yevick (PY) and hypernetted chain (HNC) closures, is appropriate for the colloids considered in this work. Defining $\nu(r) = h(r) - c_d(r)$ the RY closure can be written as

$$g(r) = \exp[\Phi(r)] \left(1 + \frac{\exp[\nu(r)\lambda(r)] - 1}{\lambda(r)} \right), \quad (2)$$

with $\Phi(r)$ the dimensionless pair interaction potential and $\lambda(r) = 1 - \exp(-\xi r)$, with ξ the RY mixing parameter. When $\xi = 0$ the closure reduces to the PY closure and when $\xi = \infty$ it reduces to the HNC closure. This parameter is determined by requiring thermodynamic consistency in matching the bulk modulus predicted by the compressibility equation

$$(kT)^{-1} \left[\frac{\partial P}{\partial C} \right]_T = 1 - C \int c_d(r)dr \quad (3)$$

and the pressure equation

$$(kT)^{-1} \left[\frac{\partial P}{\partial C} \right]_T = 1 - C \int r \frac{\partial \Phi(r)}{\partial r} g(r)dr. \quad (4)$$

As the HNC and PY equations bracket the compressibility and microstructure for repulsive and hard-sphere potentials [17,18], mixing these two integral equations generates an equilibrium structure yielding equal compressibilities from both of the above equations. The accuracy of this scheme has been demonstrated previously by comparison with Monte Carlo simulations and structure measurements [18,19].

Given the pair distribution function, the static structure factor is the Fourier transform as (with r dimensionless with particle radius a):

$$S(k) = 1 + 3\phi \int \frac{\sin kr}{kr} [g(r) - 1] r^2 dr, \quad (5)$$

where $\phi = 4\pi C a^3/3$ is the volume fraction.

B. Interaction potential

The model systems treated here are suspensions of charged Brownian particles, typically realized as suspensions of polystyrene latex particles in water. The dissociated chemical charge groups on the particle surfaces lead to an electrostatic repulsion that stabilizes the suspension. The dissociated and added salt ions are generally treated as point charges and the fluid properties, such as viscosity (η_0), dielectric constant (ϵ), and the ionic mobilities are taken to be uniform as the ion concentration is usually millimolar or less.

Solution of the linearized Poisson-Boltzmann equation for the distribution of the small ions around a macroion yield the Debye-Hückel electrostatic potential around a spherical particle [43]. This potential depends on the screening length κ , which is related to the concentration of all small ions n_k with charge z_k , including both added salt ions and the counterions from the colloids themselves, as

$$\kappa^2 = \frac{4\pi e^2}{\epsilon k_b T} \sum_k n_k (z_k)^2. \quad (6)$$

Superposition of two such interactions between spherical particles leads to an interaction potential of Yukawa form [43] (with r and κ made dimensionless with the particle radius a and the potential scaled on $k_b T$)

$$\Phi(r) = \frac{U_o}{r} e^{-\kappa(r-2)}. \quad (7)$$

The dimensionless prefactor U_o is given in terms of the colloid charge Q , and the dielectric constant of the material ϵ as [44]

$$U_o = \frac{(Qe)^2}{k_b T \epsilon (1 + \kappa a)^2}. \quad (8)$$

This potential is density dependent as the screening length varies with the counterion concentration, which itself is given by electroneutrality as the particle concentration times Q . Corrections for the nonlinear Poisson-Boltzmann equation based on a renormalized charge have been presented [45]. As recently demonstrated by Löwen [46,47], the Yukawa form provides an accurate representation of suspension microstructure if the surface charge is determined by fitting to structure measurements. In what follows, the charge is determined directly from fits of the equilibrium structure factor (when available) and this charge is used consistently throughout the formalism to calculate the dynamics and mechanical behavior of the suspension.

In this and previous work, the other colloidal forces, such as van der Waals attractions, have been neglected based on simple calculations of their relative magnitude [31]. It is straightforward to include other pairwise additive potentials within the formalism. For the systems

under consideration, the simple Yukawa interaction will dominate the other thermodynamic and hydrodynamic interactions between the particles. A more complete discussion of the role of colloidal forces in suspension rheology can be found in [48].

C. Polydispersity

As most colloidal suspensions have an appreciable amount of polydispersity, it is important to consider the effects of polydispersity within the framework of the above theory. Significant work has been done to investigate the effects of polydispersity on the equilibrium properties of Yukawa suspensions through the OZ-RY formalism, with comparable investigations of the self-diffusion dynamics [10,19,49–52]. Comparing the results to DLS and Monte Carlo simulations demonstrates the validity of the treatment. For the work considered here, polydispersity will be explicitly accounted for in the calculation of the inputs to the generalized hydrodynamics theory, i.e., the structure factor, the cumulants, and the elastic constants. These inputs will then *define* the effective fluid properties necessary for the calculation of the dynamics. No explicit treatment of the dynamics of multicomponent mixtures will be considered; however, as the generalized hydrodynamic description is derived in terms of a hydrodynamic level description of an effective one-component fluid (OCF) model, this approximation should be correct to first order.

The central quantity that must be considered is the equilibrium structure factor $S(k)$. Previous work [19,49] has derived the correct form of the structure factor within the OZ-RY scheme using the Schulz distribution as a model for the polydispersity [53], and demonstrated its accuracy [51]. The intensity measured from a scattering experiment $\langle I(k) \rangle$ is typically analyzed within the framework of an effective fluid (to within an instrument factor) as

$$\langle I(k) \rangle = C \bar{f}^2 \overline{P(k)} S^M(k), \quad (9)$$

where $\bar{f}^2 \overline{P(k)}$ is the form factor for the mixture as determined from the scattering from dilute suspensions and $S^M(k)$ is the measured structure factor. This structure factor is a convolution of both single particle and interparticle scattering and does not correspond to a thermodynamic property except in the limit of monodisperse suspensions:

$$\begin{aligned} S^M(k) &= \frac{1}{\bar{f}^2 \overline{P(k)}} \sum_{\alpha} \sum_{\beta} f_{\alpha} f_{\beta} B_{\alpha} B_{\beta} S_{\alpha\beta} \\ f_{\alpha} &= \frac{4\pi a_{\alpha}^3}{3} \\ B_{\alpha} &= \frac{3j_1(ka_{\alpha})}{ka_{\alpha}} \\ S_{\alpha\beta}(k) &= x_{\alpha} \delta_{\alpha\beta} + n x_{\alpha} x_{\beta} h_{\alpha\beta}(k) \\ h_{\alpha\beta}(r) &= c_{d,\alpha\beta}(r) \\ &+ C \sum_{\lambda=1}^p x_{\lambda} \int h_{\alpha\lambda}(r_1) c_{d,\lambda\gamma}(|\mathbf{r} - \mathbf{r}_1|) d\mathbf{r}_1. \end{aligned} \quad (10)$$

In the above j_1 is the spherical Bessel function and the particles are assumed to be of similar chemical constitution.

The structure factor that corresponds to the generalized compressibility $S^T(k)$ can be constructed from the partial structure factors as

$$S^T(k) = \frac{|\mathbf{S}(k)|}{\sum_{\alpha} \sum_{\beta} x_{\alpha} x_{\beta} |\mathbf{S}(k)|_{\alpha\beta}} = C k_b T K_T(k), \quad (11)$$

where the numerator is the determinant of the $S_{\alpha\beta}(k)$ elements, the denominator contains the cofactor of the $\alpha\beta$ element, and $K_T(k)$ is the wave vector dependent compressibility. It is this thermodynamic structure factor that is to be used in the calculation of the generalized hydrodynamics equations for polydisperse suspensions in place of $S(k)$.

The first cumulant, as it is extracted from the intensity autocorrelation function, will contain a mixture of single and interparticle scattering for a polydisperse suspension. Using the same methodology that lead to the above relations, it is can be shown that [54]

$$\langle \mu_1^c(k) \rangle^m = k^2 \frac{\sum_{\alpha} \sum_{\beta} f_{\alpha} f_{\beta} B_{\alpha} B_{\beta} D_{\alpha\beta}^o}{f^2 P(k) S^M(k)}, \quad D_{\alpha\beta}^o = \frac{k_b T}{3\pi\mu_o} \left(\frac{1}{a_{\alpha}} + \frac{1}{a_{\beta}} \right). \quad (12)$$

The second cumulant is a more complicated convolution of single and interparticle scattering, defined as

$$\langle \mu_2^c(k) \rangle^m = - \lim_{t \rightarrow 0} \frac{\partial^2}{\partial t^2} \ln S^M(k, t). \quad (13)$$

Aside from investigation of the dilute limit and experimental determination for the *self*-intermediate-scattering function [55–57], there is a scarcity of information on how to calculate this quantity for polydisperse suspensions. As previous investigations [56] have determined that polydispersity has itself only a small influence on the second cumulant (in comparison with the elasticity due to strong interparticle interaction, but again for the self-intermediate-scattering function), a different tack is taken here. In keeping with the effective fluid concept, the quantities appearing in the expression for the second cumulant for a monodisperse sample are replaced by their polydisperse equivalents; namely,

$$\langle \mu_2^c(k) \rangle^m = - \langle \mu_1^c(k) \rangle^m \frac{k^2}{C\zeta_o} \left(\langle E'_{\infty}(k) \rangle - \frac{C k_b T}{S^M(k)} \right), \quad (14)$$

where ζ_o is the hydrodynamic friction coefficient for a bare particle. This relation essentially represents a decoupling approximation, which is expected to be very reasonable for the systems considered here. These cumulants can be directly compared with DLS measurements of the cumulants.

For input into the generalized hydrodynamics equations, thermodynamic cumulants are defined as

$$\langle \mu_1^c(k) \rangle^T = k^2 \frac{\sum_{\alpha} \sum_{\beta} D_{\alpha\beta}^o}{S^T(k)}, \quad D_{\alpha\beta}^o = \frac{k_b T}{3\pi\mu_o} \left(\frac{1}{a_{\alpha}} + \frac{1}{a_{\beta}} \right), \quad (15)$$

$$\langle \mu_2^c(k) \rangle^T = - \langle \mu_1^c(k) \rangle^T \frac{k^2}{C\zeta_o} \left(\langle E'_{\infty}(k) \rangle - \frac{C k_b T}{S^T(k)} \right), \quad (16)$$

where the same decoupling approximation is used for the second cumulant as for the measured second cumulant.

The high frequency elastic constants are generalized from the Zwanzig-Mountain formulation [58] as

$$\frac{G'_{\infty}(a)^3}{k_B T} = \frac{3}{4\pi} \bar{\phi} + \frac{3}{8\pi} \sum_{i,j} \frac{\phi_i \phi_j}{(\alpha_i \alpha_j)^3} \times \int \frac{d^2 \Phi_{ij}(s)}{ds_x^2} g_{ij}(s) \frac{1 - \cos(ks_z)}{k^2} ds, \quad (17)$$

$$\frac{E'_{\infty}(a)^3}{k_B T} = \frac{9}{4\pi} \bar{\phi} + \frac{9}{8\pi} \sum_{i,j} \frac{\phi_i \phi_j}{(\alpha_i \alpha_j)^3} \times \int \frac{d^2 \Phi_{ij}(s)}{ds_x^2} g_{ij}(s) \frac{1 - \cos(ks_z)}{k^2} ds, \quad (18)$$

where $\alpha_i = \frac{a_i}{a}$, $\bar{\phi} = \frac{4\pi C(a)^3}{3}$, Φ_{ij} is the Yukawa potential between particles of type i and j , g_{ij} is the partial radial distribution function, and $s = \frac{2r}{a_{\alpha} + a_{\beta}}$. In the above equation, all hydrodynamic interactions have been neglected but can be readily included in the pairwise additive approximation (see [30,59]).

III. GENERALIZED HYDRODYNAMICS AND THE MODE-MODE-COUPLING CLOSURE

Generalized hydrodynamics provides a frequency and wave-vector generalization of the linear continuum hydrodynamic equations describing the suspension. It naturally arises when considering nonlocal relationships for the fundamental properties of molecular and complex fluids [13,1,10]. Here it is desired to obtain transport coefficients expressed entirely in terms of equilibrium suspension properties, i.e., physicochemical parameters and the structure factor. Significant development in this regard has evolved a self-consistent set of equations that express suspension dynamics entirely in terms of equilibrium properties. Coupled with the above theory for predicting the equilibrium structure in terms of fundamental parameters of the system, this program leads to a complete and consistent treatment of complex fluids in equilibrium and in the linear response regime. In what follows, the basic relations are presented and some approximate solutions discussed.

The concentration fluctuations that give rise to the time dependent diffusion and structure can be used as a basis to understand the generalized force fluctuations in suspensions. These fluctuations in stress give rise to the

viscosity, defined as the ratio of a response function for correlations in the stress fluctuations to correlations in the current fluctuations. This viscosity controls the rate of decay of the concentration fluctuations in the suspension. Mode-mode coupling projects the stress fluctuations onto the space defined in terms of bilinear products of concentration fluctuations, thus closing the equations. Thus projection operator techniques relating the stress fluctuations to the concentration and current fluctuations yield expressions for the viscosity functions in terms of the time dependent structure factor of the suspension. This approximation is expected to work if the concentration fluctuations are the slowest relaxing of the fast variables in the system. These equations are self-consistent, although they may not always yield the correct dilute limiting behavior. In what follows, hydrodynamic coupling will be neglected as the dominant effect will arise from interparticle interactions.

The correlation function of interest is the dynamic structure factor

$$S(k, t) = \frac{1}{N} \sum_{i,j=1}^N \langle \exp[i\mathbf{k} \cdot (\mathbf{r}_i(0) - \mathbf{r}_j(t))] \rangle. \quad (19)$$

This can be expressed in terms of the Fourier components of the macroparticle density

$$C(\mathbf{r}, t) = \sum_{i=1}^N \delta(\mathbf{r} - \mathbf{r}_i(t)) \quad (20)$$

as

$$\begin{aligned} S(k, t) &= \frac{1}{N} \langle C(\mathbf{k}, t) C(-\mathbf{k}, 0) \rangle \\ &= \frac{1}{N} \langle \hat{c}(\mathbf{k}, t) \hat{c}(-\mathbf{k}, 0) \rangle, \\ \hat{c}(\mathbf{k}, t) &= C(\mathbf{k}, t) - \langle C \rangle. \end{aligned} \quad (21)$$

The particle density must satisfy a continuity equation, written in terms of the particle current density $\mathbf{j}(\mathbf{r}, t)$ as

$$\frac{\partial C(\mathbf{r}, t)}{\partial t} = -\nabla \cdot \mathbf{j}(\mathbf{r}, t). \quad (22)$$

This current density satisfies a nonlocal (in both space and time) generalization of Fick's law:

$$\mathbf{j}(\mathbf{r}, t) = \int_0^t dt' \int d\mathbf{r}' \mathbf{D}(\mathbf{r} - \mathbf{r}', t - t') \nabla_{\mathbf{r}'} C(\mathbf{r}', t'). \quad (23)$$

Using Eqs. (21) and (23) to calculate the dynamic structure factor and Laplace transforming yields the generalized diffusion equation (GDE)

$$\begin{aligned} \tilde{S}(k, z) &= \frac{S(k)}{z + \tilde{D}(k, z)k^2}, \\ \tilde{D}(k, z) &= \frac{\mathbf{k} \cdot \tilde{\mathbf{D}}(\mathbf{k}, z) \cdot \mathbf{k}}{k^2}, \end{aligned} \quad (24)$$

where $\tilde{D}(k, z)$ plays the role of the memory function for the dynamic structure factor. Setting $\tilde{D}(k, z) = D_c$, the collective diffusion coefficient, recovers the local, decou-

pled solution of the ordinary Fick's law. In the time domain, Eq. (24) above has the form of a memory equation,

$$\frac{\partial S(\mathbf{k}, t)}{\partial t} = -k^2 \int_0^t dt' D(\mathbf{k}, t - t') S(\mathbf{k}, t'), \quad (25)$$

with the collective diffusion coefficient as the memory function.

The mass diffusion coefficient is directly related to the wave vector dependent, longitudinal friction coefficient via the generalized hydrodynamic relation [1]

$$D(\tilde{k}, z) = \frac{kT/[mS(k)]}{z + \tilde{\zeta}_{\parallel}(k, z)/m}. \quad (26)$$

This equation represents the generalized Stokes-Einstein relation (GSE), with $\tilde{\zeta}_{\parallel}(k, z)$ playing the role of the memory function (to be called the second memory function). The longitudinal friction coefficient is defined as

$$\begin{aligned} \tilde{\zeta}_{\parallel}(k, z) &= \frac{\mathbf{k} \cdot \tilde{\zeta}(\mathbf{k}, z) \cdot \mathbf{k}}{k^2}, \\ \tilde{\zeta}_{\parallel}(k, z) &= \zeta_o(k) + \frac{k^2}{C} \tilde{\eta}_{\parallel}(k, z). \end{aligned} \quad (27)$$

The hydrodynamic contribution ζ_o is taken to be time independent on the time scales of interest here. Again if the longitudinal friction coefficient is assumed to be constant [i.e., $\tilde{\zeta}_{\parallel}(k, z) = \zeta_o$] and in the noninteracting limit [$S(k) \rightarrow 1$] the Stokes-Einstein relation is recovered as

$$D_o = \frac{k_b T}{\zeta_o}. \quad (28)$$

In the hydrodynamic limit ($k \rightarrow 0, z \rightarrow 0$) the GSE relation reduces to

$$D_c = \frac{k_b T}{S(0)\tilde{\zeta}_{\parallel}(0, 0)} = \mu_o \frac{\partial \pi}{\partial C} \Big|_T. \quad (29)$$

Here π represents the osmotic pressure.

For systems without hydrodynamic interactions, the longitudinal dynamic viscosity is entirely due to potential interactions. Projection-operator techniques lead to the following relation for the longitudinal viscosity in terms of the interparticle stress tensor [1]:

$$\tilde{\eta}_{\parallel}(\mathbf{k}, z) = \frac{\beta}{V} \langle \hat{\sigma}_{zz}(\mathbf{k}) [z - \tilde{\Omega}\tilde{Q}]^{-1} \hat{\sigma}_{zz}(-\mathbf{k}) \rangle, \quad (30)$$

with $\tilde{\Omega}$ the Fokker-Planck operator and \tilde{Q} the orthogonal projection operator (orthogonal to the subspace spanned by current and concentration fluctuations). Closure of this set of relations requires a relationship between the interparticle contribution to the stress and the density fluctuations in the suspension.

A. Overdamped limit

For times large relative to the momentum relaxation time for the Brownian particle $\frac{m}{\zeta_o}$, the fluid of Brown-

ian particles is overdamped. As demonstrated by Hess and Klein, all Brownian systems are overdamped in the hydrodynamic limit. For such times, the generalized Stokes-Einstein relation can be reduced to

$$D(\tilde{k}, z) = \frac{kT/[mS(k)]}{\tilde{\zeta}_{\parallel}(k, z)/m}, \quad (31)$$

which can be conveniently expressed in the following form. Defining

$$\Delta D(\mathbf{k}, t) = D(\mathbf{k}, t) - D(\mathbf{k}, 0) \quad (32)$$

leads to the following memory equation in the time domain:

$$\begin{aligned} \Delta D(\mathbf{k}, t) &= \frac{D_o \mathbf{k}^4 \eta_{\parallel}(\mathbf{k}, t)}{S(\mathbf{k}) C \zeta_o} \\ &\quad - k^2 \int_0^t dt' \Delta D(\mathbf{k}, t-t') \frac{\eta_{\parallel}(\mathbf{k}, t')}{C \zeta_o}. \end{aligned} \quad (33)$$

Here $\eta_{\parallel}(\mathbf{k}, t)$ plays the role of the memory function. Also, the generalized diffusion equation (24) becomes

$$\begin{aligned} \frac{\partial S(\mathbf{k}, t)}{\partial t} &= -\frac{D_o \mathbf{k}^2}{S(\mathbf{k})} S(\mathbf{k}, t) \\ &\quad + k^2 \int_0^t dt' \Delta D(\mathbf{k}, t-t') S(\mathbf{k}, t'). \end{aligned} \quad (34)$$

Again, these equations are valid for times longer than the relaxation time of the Brownian particle's momentum. Alternately, one can start directly from the Smoluchowski dynamics and arrive at the same result [8,9].

B. Weak-coupling approximation

Before turning to the full mode-coupling approximation, it is useful to examine the exact, weak-coupling limit of this correlation function. The definition of the projection operator results in the following expression for the generalized friction coefficient [1]:

$$\begin{aligned} \Delta \zeta_{\alpha\beta}(\mathbf{k}, t) &= \frac{1}{C} k_{\gamma} k_{\delta} \eta_{\alpha\gamma\beta\delta}(\mathbf{k}, t) \\ &= \frac{1}{NkT} \left\langle \hat{f}_{\alpha}^U(\mathbf{k}) e^{\hat{\Omega}t} \hat{f}_{\beta}^U(-\mathbf{k}) \right\rangle \theta(t). \end{aligned} \quad (35)$$

The generalized force due to potential interactions $\hat{f}_{\alpha}^U(\mathbf{k})$ is given explicitly in terms of the direct force

$$\mathbf{F}_i(\mathbf{r}) = -kT \nabla_i \Phi_N(\mathbf{r}) = -kT \sum_{j(\neq i)} \frac{\partial \Phi(\mathbf{r}_i - \mathbf{r}_j)}{\partial \mathbf{r}_i}, \quad (36)$$

and the local fluctuations in concentration as

$$\hat{\mathbf{f}}^U(\mathbf{k}) = \sum_i \hat{\mathbf{F}}_i e^{-i\mathbf{k}\cdot\mathbf{r}} + kT [S(\mathbf{k})^{-1} - 1] i\mathbf{k} \hat{c}(\mathbf{k}). \quad (37)$$

In the weak-coupling approximation (WCA) the direct correlation function is replaced by the pair potential, as

$$\lim_{\Phi(\mathbf{k}) \ll 1} S(\mathbf{k}) = 1 - C\Phi(\mathbf{k}). \quad (38)$$

The WCA enables a direct reduction of the Green-Kubo form for the generalized viscosity tensor to a nonlinear integral over the dynamic structure factor. Use of Eq. (38) in (37) above yields

$$\hat{f}_{\alpha}^U(\mathbf{k}) = (2\pi)^{-3} \int d\mathbf{k}' g_{\alpha}(\mathbf{k}, \mathbf{k}') \hat{c}(\mathbf{k}'_1) \hat{c}(\mathbf{k}'_2), \quad (39)$$

where

$$\begin{aligned} \mathbf{k}'_{1,2} &= \frac{\mathbf{k}}{2} \mp \mathbf{k}', \\ g(\mathbf{k}, \mathbf{k}') &= \frac{-i}{2} [\mathbf{k}'_1 \Phi(\mathbf{k}'_1) + \mathbf{k}'_2 \Phi(\mathbf{k}'_2)]. \end{aligned} \quad (40)$$

Thus substitution of relation (39) into the friction coefficient yields

$$\begin{aligned} \Delta \zeta_{\alpha\beta}(\mathbf{k}, t) &= \frac{1}{NkT(2\pi)^6} \\ &\quad \times \int \int d\mathbf{k}' d\mathbf{k}'' g_{\alpha}(\mathbf{k}, \mathbf{k}') g_{\beta}(-\mathbf{k}, -\mathbf{k}'') \\ &\quad \times \left\langle \hat{c}(\mathbf{k}'_1) \hat{c}(\mathbf{k}'_2) e^{\hat{\Omega}t} \hat{c}(-\mathbf{k}''_1) \hat{c}(-\mathbf{k}''_2) \right\rangle \theta(t). \end{aligned} \quad (41)$$

Now, the WCA enables replacing the projected operator with the full operator, to within neglecting the first terms of order $\Phi(\mathbf{k})$. Further, the four-point correlation function is approximated by the lowest order products of two-point correlation functions as

$$\begin{aligned} &\left\langle \hat{c}(\mathbf{k}'_1) \hat{c}(\mathbf{k}'_2) e^{\hat{\Omega}t} \hat{c}(-\mathbf{k}''_1) \hat{c}(-\mathbf{k}''_2) \right\rangle \\ &\approx \left\langle \hat{c}(\mathbf{k}'_1) e^{\hat{\Omega}t} \hat{c}(-\mathbf{k}''_1) \right\rangle \left\langle \hat{c}(\mathbf{k}'_2) e^{\hat{\Omega}t} \hat{c}(-\mathbf{k}''_2) \right\rangle \\ &\quad + \left\langle \hat{c}(\mathbf{k}'_1) e^{\hat{\Omega}t} \hat{c}(-\mathbf{k}''_2) \right\rangle \left\langle \hat{c}(\mathbf{k}'_2) e^{\hat{\Omega}t} \hat{c}(-\mathbf{k}''_1) \right\rangle. \end{aligned} \quad (42)$$

Using translational invariance and the definition

$$S(\mathbf{k}, t) = \frac{1}{N} \left\langle \hat{c}(\mathbf{k}) e^{\hat{\Omega}t} \hat{c}(-\mathbf{k}) \right\rangle, \quad (43)$$

results in the final form for the longitudinal and shear viscosities as

$$\begin{aligned} \eta_{\parallel}(\mathbf{k}, t) &= \frac{2C^2}{kT(2\pi)^3} \int d\mathbf{k}' S(\mathbf{k}'_1, t) S(\mathbf{k}'_2, t) \\ &\quad \times \frac{g(k_z, k'_z) g(-k_z, -k'_z)}{k^2}, \end{aligned} \quad (44)$$

$$\begin{aligned} \eta_s(\mathbf{k}, t) &= \frac{2C^2}{kT(2\pi)^3} \int d\mathbf{k}' S(\mathbf{k}'_1, t) S(\mathbf{k}'_2, t) \\ &\quad \times \frac{g(k_x, k'_x) g(-k_x, -k'_x)}{k^2}. \end{aligned} \quad (45)$$

Results for the weak-coupling limit have been given previously for charged suspensions [1]. This result gives an exact limiting value for the strong-coupling expressions that follow.

C. Mode-mode-coupling approximation

The final step needed to close the system of equations is to express the second memory function, which has been identified as a transport coefficient [4,5,8], in terms of the dynamic structure factor. A critical part of this work involves analyzing the approximations used in formulating the mode-mode-coupling closure. This procedure involves recognizing that the slowest relaxing modes of the fast subspace will control the slow modes of the system, namely the stress fluctuations that yield the transport coefficient. A projection operator is defined to project the stress fluctuations onto bilinear products of concentration fluctuations. These bilinear products of the slowest relaxing modes of the fast subspace will be slower in relaxing than any of the fast variables. The mechanistic approximations required follow the usual paradigm [60,1,15], with the exception of the detailed treatment of three-body terms arising in the final expression. As will be shown, the two versions of the resultant expressions for the vertex, or coupling functions found in the literature

arise from different approximations used in simplifying the three-body terms.

The starting point is Eq. (30) defining the longitudinal viscosity in terms of stress fluctuations. The stress fluctuations above arise through density fluctuations as

$$\begin{aligned}\hat{\sigma}_{zz}(-\mathbf{k}) &= \hat{Q}_c \sigma_{zz}, \\ \sigma_{zz} &= \beta^{-1} \sum_{i=1}^N e^{-i\mathbf{k}\cdot\mathbf{r}_i} + k^{-2} \sum_{i=1}^N i\mathbf{k}\cdot\mathbf{F}^i e^{-i\mathbf{k}\cdot\mathbf{r}_i},\end{aligned}\quad (46)$$

with \mathbf{F}_i the direct interparticle force [61]. The projection operator is defined on the density subspace as

$$1 - \hat{Q}_c = \hat{P}_c = C(-\mathbf{k}) \frac{1}{NS(\mathbf{k})} \langle C(\mathbf{k}) \rangle. \quad (47)$$

Now the mode-coupling procedure discussed above requires a projection operator for the subspace of bilinear products of density fluctuations

$$\begin{aligned}\hat{P}_2 &= \sum_{\mathbf{k}_1} \sum_{\mathbf{k}_2} \sum_{\mathbf{k}_3} \sum_{\mathbf{k}_4} \langle C(\mathbf{k}_1) C(\mathbf{k}_2) \rangle \\ &\quad \times B^{-1}(\mathbf{k}_1 \mathbf{k}_2 \mathbf{k}_3 \mathbf{k}_4) \langle C(\mathbf{k}_3) C(\mathbf{k}_4) \rangle.\end{aligned}\quad (48)$$

Normalization such that $\hat{P}_2 \hat{P}_2 = \hat{P}_2$ determines

$$B^{-1}(\mathbf{k}_1 \mathbf{k}_2 \mathbf{k}_3 \mathbf{k}_4) = \frac{(2\pi)^6 [\delta(\mathbf{k}_1 + \mathbf{k}_3) \delta(\mathbf{k}_2 + \mathbf{k}_4) + \delta(\mathbf{k}_1 + \mathbf{k}_4) \delta(\mathbf{k}_2 + \mathbf{k}_3)]}{4C^2 S(\mathbf{k}_1) S(\mathbf{k}_2)}, \quad (49)$$

resulting in

$$\hat{P}_2 = \sum_{\mathbf{k}_1} \sum_{\mathbf{k}_2} \frac{C(\mathbf{k}_1) C(\mathbf{k}_2) \langle C(-\mathbf{k}_1) C(-\mathbf{k}_2) \rangle}{2C^2 S(\mathbf{k}_1) S(\mathbf{k}_2)}. \quad (50)$$

Note that the longitudinal stress lies fully in the subspace onto which this projects.

Now following the procedure outlined by Hess and Klein [61,1] and Szamel and Löwen [62], the longitudinal friction function is rewritten as

$$\eta_{||}(\mathbf{k}t) = \frac{\beta}{V} \left\langle \hat{\sigma}_{zz}(\mathbf{k}) \hat{P}_2 e^{\hat{\Omega}t} \hat{P}_2 \hat{\sigma}_{zz}(-\mathbf{k}) \right\rangle. \quad (51)$$

Substitution of Eq. (50) for the projection operator results in a number of higher correlations that must be evaluated. The time evolution operator occurs in the following four-point correlation function:

$$\mathcal{F}_4 = \left\langle C(-\mathbf{k}_1) C(-\mathbf{k}_2) e^{\hat{\Omega}t} C(\mathbf{k}_3) C(\mathbf{k}_4) \right\rangle. \quad (52)$$

The projected time evolution operator is replaced by its unprojected value,

$$\hat{\Omega} \hat{Q} \approx \hat{\Omega}. \quad (53)$$

Further, the four-point correlation function is factored as

$$\begin{aligned}\mathcal{F}_4 &\approx \left\langle C(-\mathbf{k}_1) e^{\hat{\Omega}t} C(\mathbf{k}_3) \right\rangle \left\langle C(-\mathbf{k}_2) e^{\hat{\Omega}t} C(\mathbf{k}_4) \right\rangle \\ &\quad \times \frac{(2\pi)^3}{V} [\delta(\mathbf{k}_1 - \mathbf{k}_3) + \delta(\mathbf{k}_2 - \mathbf{k}_4)] \\ &= S(\mathbf{k}_1, t) S(\mathbf{k}_2, t) N C(2\pi)^3 \\ &\quad \times [\delta(\mathbf{k}' - \mathbf{k}'') + \delta(\mathbf{k}' - \mathbf{k}'')], \\ &\quad \mathbf{k}_1 - \mathbf{k}_2 = \mathbf{k}', \\ &\quad \mathbf{k}_3 - \mathbf{k}_4 = \mathbf{k}''.\end{aligned}\quad (54)$$

These two assumptions constitute the usual procedure in mode-coupling analyses [60,1,15,13].

The last part of the longitudinal friction coefficient is the coupling vertex, given as

$$\langle C(\mathbf{k}_3) C(\mathbf{k}_4) \hat{\sigma}_{zz}(-\mathbf{k}) \rangle. \quad (55)$$

This can be broken into two terms through substitution of Eqs. (46) and (47) into the above. The first can be rewritten as

$$\begin{aligned}\left\langle C(\mathbf{k}_3) C(\mathbf{k}_4) \sum_{i=1}^N (i\mathbf{k}\cdot\mathbf{F}^i/k^2 - k_b T) e^{-i\mathbf{k}\cdot\mathbf{r}_i} \right\rangle \\ = \frac{-Nk_b T}{k^2} \delta[\mathbf{k} - (\mathbf{k}_3 + \mathbf{k}_4)] \\ \times [\mathbf{k}\cdot\mathbf{k}_3 S(\mathbf{k}_4) + \mathbf{k}\cdot\mathbf{k}_4 S(\mathbf{k}_3)].\end{aligned}\quad (56)$$

This term alone is unacceptable as is since it necessitates a cutoff at large wave vectors for the integration to converge.

The second part of the three-body correlation function has the form

$$\begin{aligned} \mathcal{F}_3 &= \langle C(\mathbf{k}_3)C(\mathbf{k}_4)\hat{P}_c\sigma_{zz}(-\mathbf{k}) \rangle \\ &= \left\langle C(\mathbf{k}_3)C(\mathbf{k}_4)\hat{P}_c \sum_{i=1}^N (i\mathbf{k} \cdot \mathbf{F}^i/k^2 - k_b T) e^{-i\mathbf{k} \cdot \mathbf{r}_i} \right\rangle. \end{aligned} \quad (57)$$

Inserting the definition of the projection operator, Eq. (47), into Eq. (57) above yields the following expression for this part of the three-body correlation function:

$$\begin{aligned} \frac{1}{\beta S(\mathbf{k})} \langle C(\mathbf{k}_3)C(\mathbf{k}_4)C(-\mathbf{k}) \rangle &= \frac{1}{\beta N^2 S(\mathbf{k})} \langle C(\mathbf{k}_3 + \mathbf{k}_4)C(-\mathbf{k}) \rangle \langle C(\mathbf{k}_3)C(-\mathbf{k} + \mathbf{k}_4) \rangle \langle C(\mathbf{k}_4)C(-\mathbf{k} + \mathbf{k}_3) \rangle \\ &= \frac{N}{\beta S(\mathbf{k})} S(\mathbf{k})S(\mathbf{k}_3)S(\mathbf{k}_4), \end{aligned} \quad (59)$$

which is analogous to the Kirkwood superposition approximation but in Fourier space [64]. The result of combining this with the first part, Eq. (56), is

$$\frac{-N}{\beta k^2} \delta(\mathbf{k} - (\mathbf{k}_3 + \mathbf{k}_4)) \left[\frac{\mathbf{k} \cdot \mathbf{k}_3 S(\mathbf{k}_4)(1 - S(\mathbf{k}_3)) + \mathbf{k} \cdot \mathbf{k}_4 S(\mathbf{k}_3)(1 - S(\mathbf{k}_4))}{2C^2 S(\mathbf{k}_3)S(\mathbf{k}_4)} \right]. \quad (60)$$

The result for the longitudinal friction coefficient is obtained by substitution of Eqs. (60) and (54) into (51), yielding

$$\begin{aligned} [\eta_{\parallel}(\mathbf{k}, t)]^{\text{CA}} &= \frac{2C^2\beta}{(2\pi)^3} \int d\mathbf{k}' g_{zz}^{\text{CA}}(\mathbf{k}, \mathbf{k}') g_{zz}^{\text{CA}}(-\mathbf{k}, -\mathbf{k}') S(\mathbf{k}_1, t), S(\mathbf{k}_2, t), \\ g_{zz}^{\text{CA}}(\mathbf{k}, \mathbf{k}') &= \frac{i}{2\beta k^2} (\mathbf{k} \cdot \mathbf{k}'_1 c_d(k'_1) + \mathbf{k} \cdot \mathbf{k}'_2 c_d(k'_2)), \\ \mathbf{k}'_{1,2} &= \mathbf{k}/2 \mp \mathbf{k}'. \end{aligned} \quad (61)$$

The vertex function g_{zz}^{CA} has strong coupling to low k values through the direct correlation function $c_d(\mathbf{k}) = (\mathbf{1} - S(\mathbf{k}))/CS(\mathbf{k})$. Note that in the convolution approximation the three-body terms are completely reduced to two-body terms through Eq. (59) above. The shear component of the longitudinal stress, by a similar derivation, yields

$$\begin{aligned} [\eta_s(\mathbf{k}, t)]^{\text{CA}} &= \frac{2C^2\beta}{(2\pi)^3} \int d\mathbf{k}' g_{xx}^{\text{CA}}(\mathbf{k}, \mathbf{k}') g_{xx}^{\text{CA}}(-\mathbf{k}, -\mathbf{k}') S(\mathbf{k}_1, t), S(\mathbf{k}_2, t), \\ g_{xx}^{\text{CA}}(\mathbf{k}, \mathbf{k}') &= \frac{i}{2\beta k} (k'_{1,x} c_d(k'_1) + k'_{2,x} c_d(k'_2)). \end{aligned} \quad (62)$$

This completes the closure of the generalized hydrodynamics equations by relating the second memory function, the longitudinal friction, to the dynamic structure factor and vertex functions that depend only on equilibrium, static quantities. These simplify for $\mathbf{k} = 0$ and for isotropic systems to

$$[\eta_{\parallel}(0, t)]^{\text{CA}} = \frac{k_b T C^2}{2(2\pi)^3} \int d^3 k' S(k', t)^{-2} S(k')^2 \left(c_d(k') + k'_z \frac{1}{|k'|} \frac{dc_d(k')}{d|k'|} \right)^2, \quad (63)$$

$$[\eta_s(0, t)]^{\text{CA}} = \frac{k_b T C^2}{2(2\pi)^3} \int d^3 k' S(k', t)^2 \left(\frac{k'_x k'_z}{S(k')} \right)^2 \left(\frac{1}{|k'|} \frac{dc_d(k')}{d|k'|} \right)^2. \quad (64)$$

2. Two-body treatment

Hess and Klein [1] employed a rigorous factorization of the vertex function instead of the convolution approximation employed above, which will be referred to throughout this paper as the two-body treatment (to be denoted by TB).

The starting basis is Eq. (58) above. The summations are explicitly split into two-particle sums and three-particle sums with the following result:

$$\begin{aligned}
\langle C(\mathbf{k}_3)C(\mathbf{k}_4)C(-\mathbf{k}) \rangle &= \left\langle \sum_{i=1}^N e^{-i\mathbf{k}_1 \cdot \mathbf{r}_i} \sum_{j=1}^N e^{-i\mathbf{k}_2 \cdot \mathbf{r}_j} \sum_{l=1}^N e^{i\mathbf{k} \cdot \mathbf{r}_l} \right\rangle \\
&= \left\langle N \sum_{i=1}^N e^{-i\mathbf{k}_1 \cdot \mathbf{r}_i} \sum_{\substack{l=1 \\ l \neq i}}^N e^{i(\mathbf{k}-\mathbf{k}_2) \cdot \mathbf{r}_l} \right\rangle + \left\langle \sum_{j=1}^N e^{-i\mathbf{k}_2 \cdot \mathbf{r}_j} \sum_{\substack{l=1 \\ l \neq i}}^N e^{i(\mathbf{k}-\mathbf{k}_1) \cdot \mathbf{r}_l} \right\rangle \\
&\quad + \left\langle \sum_{j=1}^N e^{-i(\mathbf{k}_1+\mathbf{k}_2) \cdot \mathbf{r}_j} \sum_{\substack{l=1 \\ l \neq j}}^N e^{i\mathbf{k} \cdot \mathbf{r}_l} \right\rangle + \langle N \rangle + \left\langle \sum_{i=1}^N e^{-i\mathbf{k}_1 \cdot \mathbf{r}_i} \sum_{\substack{j=1 \\ j \neq i}}^N e^{-i\mathbf{k}_2 \cdot \mathbf{r}_j} \sum_{\substack{l=1 \\ l \neq i, j}}^N e^{i\mathbf{k} \cdot \mathbf{r}_l} \right\rangle. \quad (65)
\end{aligned}$$

In terms of structure factors, this can be rewritten as

$$\langle C(\mathbf{k}_3)C(\mathbf{k}_4)C(-\mathbf{k}) \rangle = NC \left[h(\mathbf{k}) + h(\mathbf{k}_3) + h(\mathbf{k}_4) + \frac{1}{C} \right] + \frac{1}{N} S_3(\mathbf{k}, \mathbf{k}_3, \mathbf{k}_4), \quad (66)$$

where $h(\mathbf{k})$ is the Fourier Transform of $h(r)$ and S_3 represents the three-body correlation function which is the last term in Eq. (65) above. Combining Eq. (66) with Eq. (56), yields the following for the correlation defined as Eq. (55):

$$\begin{aligned}
\frac{N}{\beta k^2} \delta(\mathbf{k} - (\mathbf{k}_3 + \mathbf{k}_4)) \left[\frac{\mathbf{k} \cdot \mathbf{k}_3 h(\mathbf{k}_3) + \mathbf{k} \cdot \mathbf{k}_4 h(\mathbf{k}_4)}{2CS(\mathbf{k}_3)S(\mathbf{k}_4)} \right] \\
- \frac{N}{2\beta CS(\mathbf{k})S(\mathbf{k}_3)S(\mathbf{k}_4)} \left[\frac{1}{CN} S^3(\mathbf{k}, \mathbf{k}_3, \mathbf{k}_4) + h(\mathbf{k})(h(\mathbf{k}_3) + h(\mathbf{k}_4)) \right]. \quad (67)
\end{aligned}$$

This rearrangement is performed to provide a convergent vertex. As three-body correlations are difficult to calculate and require additional approximation, Hess and Klein argued in favor of neglecting the entire second term, thus leaving a tractable result containing only two-body correlation functions.

Again, using this form for the three-point correlation function results in the following for the longitudinal and shear viscosity functions:

$$\begin{aligned}
[\eta_{\parallel}(\mathbf{k}, t)]^{\text{TB}} &= \frac{2C^2\beta}{(2\pi)^3} \int d\mathbf{k}' g_{zz}^{\text{TB}}(\mathbf{k}, \mathbf{k}') g_{zz}^{\text{TB}}(-\mathbf{k}, -\mathbf{k}') S(\mathbf{k}_1, t), S(\mathbf{k}_2, t), \\
g_{zz}^{\text{TB}}(\mathbf{k}, \mathbf{k}') &= \frac{i}{2\beta k^2 S(\mathbf{k}'_1) S(\mathbf{k}'_2)} (\mathbf{k} \cdot \mathbf{k}'_1 h(k'_1) + \mathbf{k} \cdot \mathbf{k}'_2 h(k'_2)), \\
[\eta_s(\mathbf{k}, t)]^{\text{TB}} &= \frac{2C^2\beta}{(2\pi)^3} \int d\mathbf{k}' g_{xx}^{\text{TB}}(\mathbf{k}, \mathbf{k}') g_{xx}^{\text{TB}}(-\mathbf{k}, -\mathbf{k}') S(\mathbf{k}_1, t), S(\mathbf{k}_2, t), \\
g_{xx}^{\text{TB}}(\mathbf{k}, \mathbf{k}') &= \frac{i}{2\beta k S(\mathbf{k}'_1) S(\mathbf{k}'_2)} (\mathbf{k}'_{1,x} h(k'_1) + \mathbf{k}'_{2,x} h(k'_2)). \quad (68)
\end{aligned}$$

This form, in contrast to the convolution approximation, results in a slightly more complex coupling for the vertex function. The two wave vectors are mixed to a greater degree than in the former case. Notice also that both forms reduce, in the limit of weak-coupling to the exact weak-coupling limit [Eq. (45)]. This comparison is reminiscent of the various methods of closing three-body correlation functions in equations for the equilibrium structure. As there does not seem to be any fundamental reason to choose one form over the other, the results of using both

forms in a numerical calculation will be performed to determine their performance.

These simplify for $\mathbf{k} = 0$ and for isotropic systems to

$$\begin{aligned}
\eta_{\parallel}(0, t)^{\text{TB}} &= \frac{k_b T C^2}{2(2\pi)^3} \int d^3 k' [S(k', t)]^2 [S(k')]^{-4} \\
&\quad \times \left(h(k') + k'_z \frac{1}{|k'|} \frac{dh(k')}{dk'} \right)^2, \quad (69)
\end{aligned}$$

$$\eta_s(0, t)^{\text{TB}} = \frac{k_b T C^2}{2(2\pi)^3} \int d^3 k' [S(k', t)]^2 \times \left(\frac{k'_x k'_z}{S(k')^2} \right)^2 \left(\frac{1}{|k'|} \frac{dh(k')}{d|k'|} \right)^2. \quad (70)$$

Thus, the stress relaxation functions are expressed solely in terms of the time- and wave-vector dependent structure $S(k, t)$.

D. Corrections for the zero-time limit

It is known that the mode-mode coupling (MMC) approximation is more accurate in describing the time evolution of the dynamic friction function than the initial, zero time value, which is an equilibrium property of the suspension calculable from mechanical [29,31,59] and fluctuation dissipation [58,13,59] derivations. Thus it is preferable to use the MMC approximation to calculate only the relaxation or time dependence of the dynamic friction functions and rely on the exact calculations for the initial prefactor. The relaxation functions are defined as

$$\begin{aligned} \tau_{\parallel}(\mathbf{k}, t) &= \frac{\eta_{\parallel}(\mathbf{k}, t)}{\eta_{\parallel}(\mathbf{k}, 0)}, \\ \tau_s(\mathbf{k}, t) &= \frac{\eta_s(\mathbf{k}, t)}{\eta_s(\mathbf{k}, 0)}. \end{aligned} \quad (71)$$

The correct longitudinal and shear friction functions are written in terms of the high frequency elastic constants [13]

$$\begin{aligned} \eta_{\parallel}(\mathbf{k}, 0) &= E'_{\infty}(\mathbf{k}), \\ \eta_s(\mathbf{k}, 0) &= G'_{\infty}(\mathbf{k}). \end{aligned} \quad (72)$$

This leads to the following relations based on the above definitions:

$$\begin{aligned} \eta_{\parallel}(\mathbf{k}, t) &= E'_{\infty}(\mathbf{k}) \tau_{\parallel}(\mathbf{k}, t), \\ \eta_s(\mathbf{k}, 0) &= G'_{\infty}(\mathbf{k}) \tau_s(\mathbf{k}, t). \end{aligned} \quad (73)$$

Note that this scheme takes advantage of the known, exact initial values without compromising the integrity of the MMC approximation for the dynamics.

The macroscopic dynamic properties of the suspension, such as the rheology, can then be directly calculated in terms of these dynamic friction coefficients. For example, as shown in Appendix A, the definition of the Newtonian shear viscosity yields

$$\begin{aligned} \eta_s &= \int_0^{\infty} \eta_s(0, t) dt = \int_0^{\infty} G(t) dt, \\ \eta_{\parallel} &= \int_0^{\infty} \eta_{\parallel}(0, t) dt = \int_0^{\infty} G_{\parallel}(t) dt, \end{aligned} \quad (74)$$

where $G(t)$ is the shear viscosity relaxation function discussed in Appendix A. Thus measurement of the frequency dependent viscosity or modulus can be directly compared to the time dependent viscosity function determined from generalized hydrodynamics via Fourier transforming the dynamic friction function with respect to

time. All the rest of the linear viscoelastic functions can be determined directly in this way, as demonstrated in Appendix A.

The above system of coupled integral equations can, in principle, be solved self-consistently for the dynamic structure, mass diffusion, and parallel viscosity, and then the shear viscosity calculated. In practice this has not been accomplished, but rather, three approximate techniques have been used to decouple the equations. Previous calculations based on this formalism have resulted in the following conceptual picture of suspension dynamics [1]. Strong interparticle interactions result in an overdamped system with short-range order. Relaxations are characterized by a wave vector and time dependent viscosity. The short-range order, thought of as clusters with characteristic lifetimes, govern the time dependence of this viscosity. Thus at short-times the system has elasticity, but flows as a viscous fluid at long times. The length scale being probed is also important in determining this time scale, thus the wave vector dependence. Strong coupling between concentration and stress fluctuations results in viscoelastic behavior.

IV. RESULTS AND DISCUSSION

A. Short-time approximation

The simplest method of solving the generalized hydrodynamics MMC hierarchy has been to approximate the time and wave vector dependent structure factor by a short-time (ST) expression [6,1]. This essentially decouples the hierarchy and permits calculation of the rheological properties in terms of the static structure factor and the single particle diffusion coefficient. Lindsay *et al.* [20] predicted the Maxwell relaxation time, relating the steady shear viscosity to the high frequency modulus as $\tau_s^M = \eta_s / G'_{\infty}$, to have a form similar to a Lindemann melting criterion. Here a similar approach is used to predict the frequency dependent complex shear viscosity and comparison is made with a common model for the relaxation spectrum.

In the short-time approximation the memory function for the GDE relation is neglected and the original Fick's law is maintained. The dynamic structure factor is of single exponential form with a wave vector dependent relaxation time as given by the collective diffusion coefficient:

$$[S(\mathbf{k}, t)]^{\text{ST}} = S(\mathbf{k}) \exp[-D_c(\mathbf{k}) k^2 t]. \quad (75)$$

The generalized mass or collective diffusion coefficient is written as

$$D_c(\mathbf{k}) = D^0 H(\mathbf{k}) / S(\mathbf{k}). \quad (76)$$

For the strongly charged system considered here hydrodynamic interactions will be neglected in these calculations and so the generalized sedimentation coefficient $H(\mathbf{k})$ appearing above reduces to unity. Recent calculations by Genz and Klein [65] have demonstrated the importance of including hydrodynamic interactions,

treated via the renormalization of Beenakker [66], for weakly charged suspensions. Mathematically, this form for $[S(\mathbf{k}, t)]^{\text{ST}}$ follows from replacing the fully time and wave vector dependent diffusion coefficient in the generalized diffusion equation (34) with its time integral, the collective diffusion coefficient. The physical argument is that collective concentration relaxation would occur on a time long enough that it would sample this net mass diffusion rate. In essence, this neglects memory effects and would be the result from neglecting coupling between stress and concentration fluctuations in the formalism.

With the above approximation the viscosity functions equations (63) and (64) or (69) and (70) are readily calculated from knowledge only of the static structure factor. Lindsay *et al.* [20] give typical solutions for the time dependence of the shear and longitudinal viscosities for very dilute, charged systems of spherical particles within the two-body treatment. These were then integrated, yielding the steady shear viscosity from Eq. (74). Over a dilute range of concentrations it was determined that

$$\eta_s = G'_\infty \frac{(0.1\bar{d})^2}{D_0}, \quad (77)$$

where \bar{d} is the average spacing between particles. The proportionality between the shear viscosity and the high-frequency modulus defines the Maxwell relaxation time for the system, the mean relaxation time for the stress fluctuations. The above relation is interpreted within a cage-melting picture to express an idea similar to the well known Lindemann melting criterion. Namely, the viscosity is proportional the force acting on a test particle, surrounded by an instantaneous configuration of neighbors times a relaxation time. The characteristic time required for this force to relax is given by the time necessary for the test particle to travel about one-tenth the average neighbor separation distance. This is the time necessary for the surrounding cage to “melt,” hence the analogy.

Direct Fourier transformation of the zero-wave-vector expression for the time dependent viscosity [Eqs. (70) and (74)] yields the complex, frequency dependent shear viscosity as

$$\frac{\eta_s(\omega)}{\eta_s(0)} = \frac{\int dk' S(k')^{-2} \left(k'^2 \frac{dh(k')}{dk'}\right)^2 \left(\frac{\alpha+i\omega}{\alpha^2+\omega^2}\right)}{\int dk' \frac{1}{S(k')^2 \alpha} \left(k'^2 \frac{dh(k')}{dk'}\right)^2}, \quad (78)$$

$$\alpha = \frac{2D_0 k'^2}{S(k')},$$

where ω is nondimensional with α^2/D_0 . The equivalent results within the convolution approximation can be directly obtained by substituting $c_d(k)$ for $h(k)$ and canceling $[S(k)]^{-2}$ from the integrand. Results for $S(k)$ are given in Fig. 1 for the three systems listed in Table I. The corresponding shear and longitudinal viscosities are shown in Figs. 2(a) and 2(b) for the two-body vertex functions. These rheological functions are characteristic of a linear viscoelastic fluid with a dominant Maxwell relaxation time, although there is evidence of multiple relaxation times in the broadening of the longitudinal

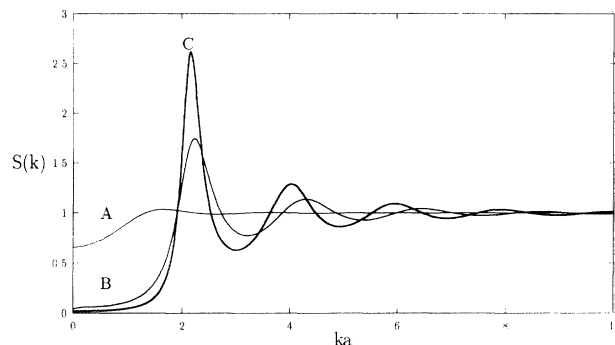


FIG. 1. Equilibrium microstructures $S(k)$ versus ka , systems A, B, and C as marked.

viscosity. Table II shows the results for these mean Maxwell relaxation times for both vertex functions and both shear and longitudinal modes. As shown, the convolution approximation yields slightly longer times and as will become more apparent in the fully self-consistent solution, always yields longitudinal relaxation times greater than for shear modes. Notice how the two-body treatment of the vertex functions leads to a longitudinal relaxation time that decreases with increasing structure (examine systems A and B), while the convolution treatment yields the opposite results. Comparison with the Lindemann criterion is quite good, with the deviation increasing as the structure factor increases. For comparison, the results of a calculation using a nonequilibrium Smoluchowski analysis is included [31], which demonstrates that this technique gives comparable results to the short-time ansatz considered here.

Given the static structure factor for suspensions of charged particles, the measurable viscosity is directly calculable in terms of the fundamental physicochemical properties of the microscopic constituents of the suspension and the solvent properties. Transformation into a relaxation spectrum yields insight into the physical processes behind the mechanical behavior. For this example of short-time behavior, the relaxation spectrum can be discerned by direct comparison of the integrands in Eq. (78) and the definitions, Eqs. (A12) and (A13), yielding

$$H(\lambda) \propto k^2 S(k) \left(\frac{dh(k)}{dk}\right)^2 \left(2\frac{S(k)}{k} - \frac{dS(k)}{dk}\right)^{-1},$$

$$\lambda = \frac{S(k)}{2D_0 k^2}. \quad (79)$$

In this case, the results for the convolution approximation can be obtained by simply multiplying the above relation by $1/[S(k)^2]$. Thus in the short-time approxi-

TABLE I. System parameters.

System	Radius (nm)	Charge (e)	Volume frac.	Added salt conc. (mM)
A	62.5	1240	0.117	0.3
B	62.5	1240	0.117	0.6
C	62.5	1240	0.01	0.3

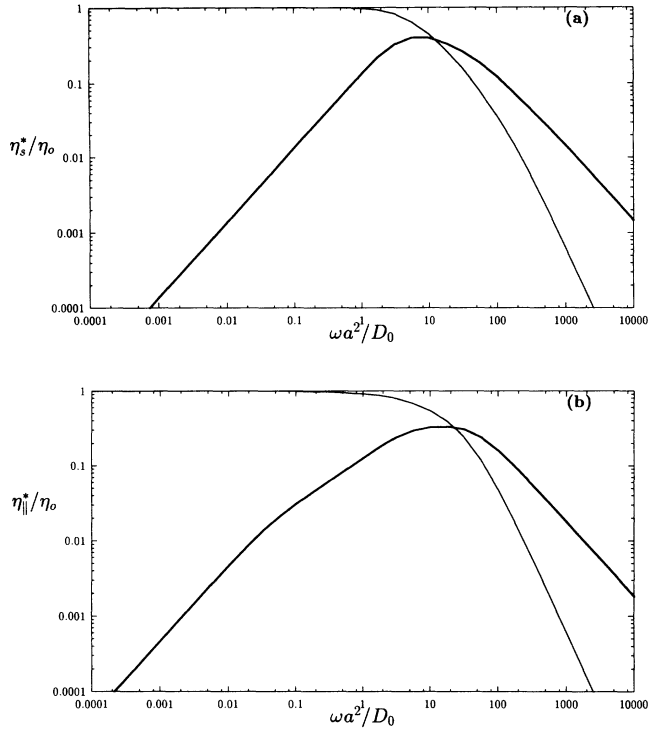


FIG. 2. Normalized frequency-dependent viscosity for system A, (a) dynamic shear viscosity, dimensionless on η_0 , (b) dynamic longitudinal viscosity, dimensionless on $\eta_{\parallel,0}$.

mation the relaxation spectrum is given entirely by the static structure factor. A quantitative result for system C (see Table I) is given in Fig. 3, where it is seen that the convolution approximation yields a longer and stronger main relaxation peak. The form of the function suggests the limitations of interpreting the short-time approximation in terms of a spectrum of Maxwell relaxation times as $H(\lambda)$ has a clear physical significance. The denominator has zeros and goes negative if $\frac{dS(k)}{dk} > 2\frac{S(k)}{k}$, which can occur if $S(k)$ has significant structure. Further, the function can be multiple valued as k itself is not a unique function of λ if $S(k)$ has significant structure. Nevertheless, the short-time calculations for the viscosity are independent of this model and are well behaved even for strongly correlated systems. The limitations on the validity of its application are determined by the neglect of the memory term.

The general asymptotic behavior of the complex viscosity is readily discernible from the above expressions. In the limit of zero frequency, the real part yields the

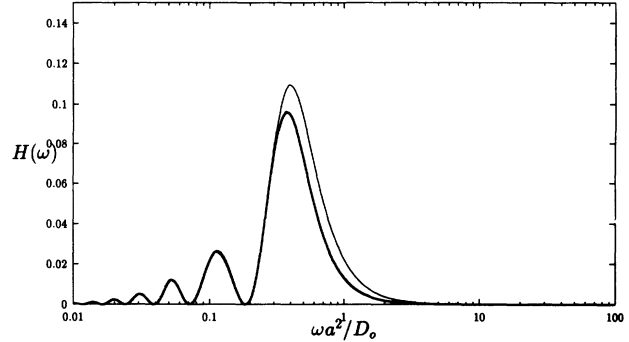


FIG. 3. Maxwell relaxation spectrum for the short-time approximation, system C, convolution approximation (thin line), two-body approximation (thick line).

steady shear viscosity; it decreases as the frequency squared in the high frequency limit. The imaginary part is proportional to the frequency in this limit. For infinite frequencies, the loss part decays as inverse frequency squared while the storage part goes inversely with the frequency [see Eq. (A13)]. Accounting for the direct hydrodynamic contribution to the stress would yield a frequency independent contribution to the loss part of the viscosity [30]. This general behavior conforms to the notions for a simple viscoelastic material. Further, one can make an estimate of the mean relaxation time directly from the relaxation spectrum above. The dominant contribution will be at or near the peak in the structure factor, where $k_{\max} \approx 2\pi/\bar{d}$. This results in $\lambda \approx (\bar{d}/2\pi)^2 S(k_{\max})D_0$, which corresponds to the calculation of Lindsay *et al.* [20] to within an order one constant.

B. Viscoelastic approximation

A more sophisticated approximation to the generalized hydrodynamics MMC equations that maintains the self-consistency is the viscoelastic approximation (VEA). This is physically motivated by trying to approximate the time behavior of the system by an interpolation between short-time elasticity and long-time fluid behavior. For “short” times (on the diffusion time scale) the suspension behaves like an elastic solid while for “long” times the suspension will flow like a fluid. Thus the approximation defines generalized Maxwell relaxation times for the shear and longitudinal viscosities and approximates the time dependence of the generalized mass diffusivity as a

TABLE II. Maxwell relaxation times. TB refers to the two-body vertex functions, CA to the convolution approximation, and SE denotes the results of the Smoluchowski equation in Ref. [31].

System	$\tau_s^M \left(\frac{\alpha^2}{D_0} \right)$			Lindemann	$\tau_{\parallel}^M \left(\frac{\alpha^2}{D_0} \right)$	
	ST-TB	ST-CA	SE		ST-TB	ST-CA
A	0.068	0.069	0.076	0.042	0.055	0.075
B	0.060	0.061	0.051	0.042	0.099	0.063
C	0.23	0.23	0.26	0.22	0.83	0.51

simple exponential decay [1]. Alternately, one can consider this as a model for the second memory function, the memory function for the GSE relation [1,8,9]. The VEA replaces the full wave vector and time dependent memory function with a single exponential containing a time constant that is wave vector dependent. However, unlike the previous models for the memory function, this approximation does not specify the wave vector dependence explicitly; it is to be determined by the self-consistent solution of the generalized hydrodynamic equations.

Mathematically, the above assumption translates into the statement

$$\Delta\hat{\zeta}_{\parallel}(\mathbf{k}, z) \approx \frac{\Delta\zeta_{\parallel}(\mathbf{k}, 0)}{z + [\tau_{\parallel}^M(\mathbf{k})]^{-1}}, \quad (80)$$

defining the Maxwell relaxation time for longitudinal friction. This can also be calculated, in the absence of hydrodynamic interaction, from the contribution of interparticle interaction to the longitudinal viscosity

$$\tau_{\parallel}^M(\mathbf{k}) = \frac{1}{\eta_{\parallel}(\mathbf{k}, 0)} \int_0^{\infty} dt \eta_{\parallel}(\mathbf{k}, t) = \frac{\hat{\eta}_{\parallel}(\mathbf{k}, z=0)}{\eta_{\parallel}(\mathbf{k}, 0)}, \quad (81)$$

where $\Delta\hat{\zeta}_{\parallel}(\mathbf{k}, z) = k^2 \Delta\hat{\eta}_{\parallel}(\mathbf{k}, z)/(C\zeta_0)$. Substitution into the GSE (31) leads to a single exponential for the time dependent part of the generalized mass diffusivity in the overdamped limit,

$$\begin{aligned} \Delta\hat{D}(\mathbf{k}, z) &= D^{\infty}(\mathbf{k}) \frac{\Delta\hat{\zeta}_{\parallel}(\mathbf{k}, z)}{\zeta_{\parallel}^{\infty}(\mathbf{k}) + \Delta\hat{\zeta}_{\parallel}(\mathbf{k}, z)} \\ &\approx \frac{-\mu_2(\mathbf{k})/k^2}{z + (\tau_{\parallel}^M(\mathbf{k}))^{-1}}. \end{aligned} \quad (82)$$

This single exponential ansatz defines the Maxwell relaxation time for diffusion as

$$(\tau_D^M(\mathbf{k}))^{-1} = (\tau_{\parallel}^M(\mathbf{k}))^{-1} - \frac{\mu_2(\mathbf{k})}{\mu_1(\mathbf{k})},$$

$$\Delta D(\mathbf{k}, t) = D^{\infty}(\mathbf{k}) - D(\mathbf{k}, t) = -\frac{\mu_2(\mathbf{k})}{k^2} e^{-t/\tau_D^M(\mathbf{k})} \theta(t). \quad (83)$$

Direct substitution into the overdamped GDE, Eq. (34), leads to two poles resulting in a double exponential form for the dynamic structure factor:

$$\begin{aligned} \frac{S(\mathbf{k}, t)}{S(\mathbf{k})} &= a(\mathbf{k}) e^{-t/\tau_1(\mathbf{k})} + (1 - a(\mathbf{k})) e^{-t/\tau_2(\mathbf{k})}, \\ (\tau_{1,2}(\mathbf{k}))^{-1} &= \frac{1}{2} \left[\mu_1(\mathbf{k}) + (\tau_D^M(\mathbf{k}))^{-1} \right] \\ &\quad \pm \left[\frac{1}{4} \left[\mu_1(\mathbf{k}) - (\tau_D^M(\mathbf{k}))^{-1} \right]^2 - \mu_2(\mathbf{k}) \right]^{1/2}, \\ a(\mathbf{k}) &= \frac{1}{2} + \frac{\mu_1(\mathbf{k}) - (\tau_D^M(\mathbf{k}))^{-1}}{2 \left[\left[\mu_1(\mathbf{k}) - (\tau_D^M(\mathbf{k}))^{-1} \right]^2 - 4\mu_2(\mathbf{k}) \right]^{1/2}}. \end{aligned} \quad (84)$$

The mean structural relaxation time is given by

$$\tau_{S(k)}^m(k) = a(k)\tau_1(k) + (1 - a(k))\tau_2(k). \quad (85)$$

The three parameters $a(k), \tau_{1,2}(k)$ are then algebraically related to the mean diffusion and longitudinal viscosity relaxation times as

$$\begin{aligned} \tau_D^M(\mathbf{k}) &= \frac{\tau_1(\mathbf{k})\tau_2(\mathbf{k})}{a(\mathbf{k})\tau_1(\mathbf{k}) + (1 - a(\mathbf{k}))\tau_2(\mathbf{k})}, \\ \tau_{\parallel}^M(\mathbf{k}) &= a(\mathbf{k})\tau_2(\mathbf{k}) + (1 - a(\mathbf{k}))\tau_1(\mathbf{k}). \end{aligned} \quad (86)$$

The result is a closed set of nonlinear equations that are simpler than the more general set but still formidable. Because of the viscoelastic approximation, one might expect to predict the correct overall behavior but not capture all of the details of the relaxation processes from this approach.

1. Weak-coupling limit of the viscoelastic approximation

Examination of Eq. (84) shows that the group under the square root can be viewed as the strength of the coupling between the elasticity of the suspension and the density fluctuations. In the limit that of weak coupling the second cumulant is small, $\mu_2^c \rightarrow 0$ implying no elasticity and low concentrations,

$$\frac{-4\mu_2^c}{(\mu_1^c - \tau_D^{M^{-1}})^2} \ll 1. \quad (87)$$

The two modes are then given by

$$\begin{aligned} \tau_1 &= \mu_1^{c^{-1}}, \\ \tau_2 &= \tau_{\parallel}^M, \\ a(k) &= 1. \end{aligned} \quad (88)$$

The two modes are completely decoupled, the first being pure spatial diffusion as given by the short-time solution. The mass diffusivity relaxes purely by the longitudinal friction and the dynamic structure factor is given by a single exponential equivalent to the short-time solution.

This solution is also necessarily true for all conditions in the limit as $k \rightarrow 0$, as can be seen from the hydrodynamic limiting behavior of the cumulants. In the hydrodynamic limit μ_2^c goes to zero as k^4 while μ_1^c goes as k^2 , leading to the above condition. This is required so that $\tau_{\parallel}^M(k=0)$ can remain finite, which is necessary for the collective diffusivity to go to its correct hydrodynamic limit, while the relaxation time of the density fluctuations in the hydrodynamic limit goes to infinity.

2. Strong coupling limit of the viscoelastic approximation

In previous work [1] the square root was expanded to yield the following relations for small amounts of coupling:

$$\begin{aligned} \tau_1^{-1} &= \mu_1^c - \frac{\mu_2^c}{\mu_1^c - \tau_D^{M^{-1}}}, \\ \tau_2^{-1} &= (\tau_D)^{M^{-1}} - \frac{\mu_2^c}{\mu_1^c - \tau_D^{M^{-1}}}, \\ a(k) &= 1 + \frac{\mu_2^c}{(\mu_1^c - \tau_D^{M^{-1}})^2}. \end{aligned} \quad (89)$$

This leads to further separation of frequencies, implying faster concentration fluctuations and diffusion for $\mu_1^c > \tau_D^{M-1}$. For the opposite case, the diffusion relaxation frequency becomes smaller. The weighting of the relaxation times now begins to mix in the viscoelastic character of the longitudinal friction.

Taking the opposite limit, the strong coupling limit of

$$\frac{-4\mu_2^c}{(\mu_1^c - \tau_D^{M-1})^2} \gg 1 \quad (90)$$

was analyzed to yield

$$\begin{aligned} \tau_{1,2}^{-1} &= \frac{1}{2}(\mu_1^c - \tau_D^{M-1}) \pm (-\mu_2^c)^{\frac{1}{2}}, \\ a(k) &= \frac{1}{2}. \end{aligned} \quad (91)$$

This leads to two, mixed modes that are not clearly separable as to their physical origin.

However, analysis of this limit proves it to be unattainable for physically realistic colloidal suspensions. Substitution of the above relation (91) into the equation for the diffusional relaxation time (86) yields

$$\tau_D^{M-1} = \mu_1^c, \quad (92)$$

which satisfies relation (90) automatically. In this limit, relation (86) becomes

$$\begin{aligned} \tau_{\parallel}^{M-1} &= \tau_D^{M-1} - \frac{-\mu_2^c}{\mu_1^c} \\ &= \mu_1^c - \frac{-\mu_2^c}{\mu_1^c}. \end{aligned} \quad (93)$$

As τ_{\parallel}^{M-1} must be real positive for a Brownian fluid, the inequality $\frac{-\mu_2^c}{(\mu_1^c)^2} < 1$ must be satisfied. However, the second cumulant written in nondimensional form becomes

$$\mu_2^c = -(\mu_1^c)^2 \left[S(k) \frac{4\pi}{3\phi} \frac{E'_{\infty}(k)a^3}{k_b T} - 1 \right]. \quad (94)$$

In the dilute limit, $\frac{E'_{\infty}a^3}{k_b T} \rightarrow \frac{9\phi}{4\pi}$ and $S(k) \rightarrow 1$ and so $\mu_2 \rightarrow -2(\mu_1^c)^2$ violating the above inequality. The situation becomes worse with increasing concentration, leading to no physically realizable solution in this limit.

There is another strong-coupling limit that can be obtained from direct consideration of the slowing down of the longitudinal stress fluctuations. For strongly interacting systems it is expected that the Maxwell relaxation time for longitudinal stress fluctuations becomes large ($\tau_{\parallel}^M \rightarrow \infty$) due to the interactions. Equally valid is the picture of strong longitudinal elasticity, such that $-\mu_2^c/\mu_1^c$ becomes relatively large. In this limit, the diffusional relaxation time becomes

$$\begin{aligned} \tau_D^{-1} &= \tau_{\parallel}^{M-1} + \frac{-\mu_2^c}{\mu_1^c} \\ &\approx \frac{-\mu_2^c}{\mu_1^c}. \end{aligned} \quad (95)$$

This immediately results in the limiting behavior

$$\begin{aligned} \tau_1 &= \frac{\mu_1^c}{(\mu_1^c)^2 - \mu_2^c}, \\ a(k) &= \mu_1^c * \tau_1. \end{aligned} \quad (96)$$

Further τ_2 is seen to become proportional to τ_{\parallel}^M through relation (86) and both are large. As discussed above, these relations must have the proper hydrodynamic limit. For $k \rightarrow 0$, τ_1 diverges proportional to μ_1^{c-1} and the product $a(k)\tau_1$, which equals the mean structural relaxation time [see Eq. (85)], reduces to the short-time solution. Also in this limit τ_2 and τ_{\parallel}^M remain proportional and do not diverge as $k \rightarrow 0$ for a fluid. Therefore, in the strong-coupling limit the structural relaxation times become widely separated. For $k \gg 0$, τ_1 becomes small for large longitudinal elasticity while τ_2 becomes comparable to the longitudinal relaxation time. Further, the diffusion process is driven by the longitudinal elasticity $\tau_D^{-1} \approx \frac{-\mu_2^c}{\mu_1^c}$, which is expected to become small for strong coupling. The physical picture is that finite wavelength concentration fluctuations are correlated because of the elasticity arising from strong interactions between Brownian particles, resulting in both a long decay time for the dynamic structure function $S(k, t)$ and the stress relaxation as characterized by τ_{\parallel}^M .

C. Comparison with experiment

Recently, the microstructure, density fluctuation correlations, and rheology of a well characterized suspension of charged, polystyrene spheres have been measured via small-angle neutron scattering (SANS), static and dynamic light scattering (SLS, DLS), and mechanical spectrometry over a wide range of particle and added salt concentrations [50,67]. This experimental database provides a check of the above theoretical predictions by direct comparison of the microstructure, density fluctuations, and rheological predictions for systems where the equilibrium structure and the colloidal interaction parameters are well characterized. In the following, comparison of the predictions for and measurements of the intermediate scattering function will be made for dilute, but strongly correlated suspensions for which DLS is possible but mechanical spectrometry unfeasible. Then, a similar comparison of mechanical properties will be made for more concentrated systems with added salt, where DLS cannot be used to measure the intermediate scattering function but SANS and mechanical spectrometry yield the equilibrium structure and the linear rheological response.

1. Dilute samples investigated via DLS

The relaxation of the dynamic structure factor (intermediate scattering function) for a dilute but strongly correlated suspension of colloidal particles was measured with dynamic light scattering [50]. Briefly, polydisperse polystyrene spheres (number average radius 35.5 nm, number average charge $Q=390$) were suspended in deionized water at various volume fractions. DLS measure-

ments of the intensity autocorrelation function were analyzed to obtain the cumulants and the full decay of the dynamic structure factor $S(k, t)$. At each scattering wave vector, the time decay of $S(k, t)$ was fit to the double exponential form derived in the viscoelastic ansatz, Eq. (84), via a nonlinear optimization routine. It was found that the double exponential ansatz is an excellent representation of the data, as concluded from both the quality of the fit and the excellent agreement between the first and second cumulants determined from traditional polynomial fits and from the double-exponential fit. More details of the experiments and data extraction can be found in Ref. [50]. Table III provides a summary of the necessary properties measured for the suspensions.

Calculation of the equilibrium structure factors from the multicomponent OZ-RY equation were performed and excellent agreement obtained for the measured structure factors as compared to static light scattering measurements [50], verifying the validity of the approach. The polydispersity was modeled as a discretization of a Schulz distribution with $\bar{r}_{\text{mean}} = 35.0 \text{ nm} \pm 16\%$. This technique for modeling the particle distribution provides a tractable and accurate method of handling the polydispersity in particle size and charge (the surface charge density is assumed constant). Figure 4 provides an overall picture of the DLS samples' structures, where the calculated *thermodynamic* structure factor is plotted, not the measured structure factor. As seen, the structure grows smoothly with increasing concentration, with the main peak growing in magnitude along with higher order peaks. As the main peak height does not exceed 2.85, it is expected from the Hansen-Verlet criterion [68], and is indeed observed to be true, that these suspensions are fluids at rest.

The elastic moduli calculated from the polydisperse equations (17) and (18) are shown in Fig. 5. Calculations for the DLS samples results in a power law with index 1.3 for the shear modulus and 0.97 for the longitudinal

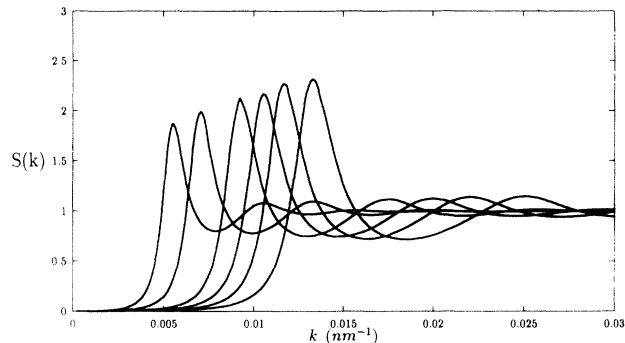


FIG. 4. Thermodynamic structure factors $S(k)$ versus k in nm^{-1} , systems RY2, RY3, RY5, RY6, RY7, RY8 correspond to the primary maximum left to right, respectively.

modulus for the variation with particle concentration. This compares well with calculations for monodisperse suspensions, where power law behavior of around 4/3 is predicted for the shear modulus [6,31]. This power law index is less than 2, reflecting the increasing counterion concentration accompanying the increasing particle concentration that decreases the screening length. Note that at these particle concentrations it is found that including hydrodynamic interactions (known for pair interactions) yields an insignificantly small quantitative change.

The static structure predictions, particle size determination, polydispersity corrections, and longitudinal elasticity can be checked by measuring the the first two cumulants. The *measured* first and second cumulants calculated according to the polydisperse equations (12) are compared against the cumulants extracted from the DLS

TABLE III. Sample characteristics.				
System	ϕ	Radius (nm)	C_{salt} (millimolar)	Q (e)
SANS samples				
1A	0.181	35.5 ± 5.7	1.0 (dialyzed)	340
1B	0.10	35.5 ± 5.7	1.0 (dialyzed)	420
1C	0.208	35.5 ± 5.7	1.0 (dialyzed)	300
2A	0.06	35.5 ± 5.7	0.1 (dialyzed)	390
2B	0.092	35.5 ± 5.7	0.1 (dialyzed)	390
2C	0.119	35.5 ± 5.7	0.1 (dialyzed)	340
3C	0.285	35.5 ± 5.7	0.01	300
4A	0.353	35.5 ± 5.7	10.0 (dialyzed)	300
SLS and DLS samples				
RY2	0.01 %	35.5 ± 5.7	deionized	390
RY3	0.0205 %	35.5 ± 5.7	deionized	390
RY5	0.047 %	35.5 ± 5.7	deionized	390
RY6	0.07 %	35.5 ± 5.7	deionized	380
RY7	0.095 %	35.5 ± 5.7	deionized	400
RY8	0.14 %	35.5 ± 5.7	deionized	390

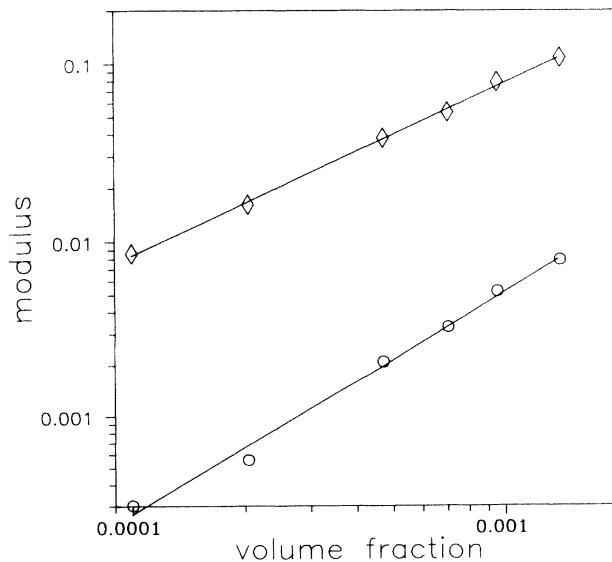


FIG. 5. High-frequency shear modulus $\frac{G'_{\infty}(\alpha)^3}{k_b T}$ (\circ) and high-frequency elastic modulus $\frac{E'_{\infty}(\alpha)^3}{k_b T}$ (\diamond) versus volume fraction for the DLS samples. The lines are best power law fits; see text.

in Figs. 6(a) and 6(b). Details of corrections for the primary electroviscous effect are treated in Appendix B. The agreement with experiment is excellent, especially around wave vectors corresponding to the peak in the structure factor, further verifying the validity of the polydisperse OCF model in accurately modeling the suspension. The variation in the second cumulant at high wave vectors can be attributed to both low signal to noise ratios and the fitting procedure used to extract the cumulants.

Both the short-time (ST) (75) and viscoelastic (VE) (83) and (84) closures for the GH equations were solved for the effective fluid using both the two-body (68) and convolution approximation (61) for the vertex functions. As inputs to the solution, the first and second cumulants [the *thermodynamic* cumulants given by Eq. (16)] and the thermodynamic structure factor (11) are calculated. This definition of an effective fluid is a consistent method to incorporate polydispersity within the philosophy of generalized hydrodynamics. Briefly, the self-consistent equations were solved iteratively by using the short-time solution (75) as an initial guess. First, the Maxwell relaxation time was calculated from the mode-mode-coupling closure to the Green-Kubo relation for the longitudinal viscosity (81). Then, the Maxwell time for collective diffusion and the two exponentials and weighting factor for the dynamic structure factor (84) were cal-

culated. These were then used to recalculate the Maxwell relaxation time for longitudinal viscosity. This procedure was performed until a mean-square deviation of less than 0.1% was achieved, which was determined to be sufficient to insure convergence. Longer ranges of integration and finer discretizations of the numerical integrations were performed until no change was observed in the final solution. As the equations are nonlinear, attempts were also made to use different starting guesses to seek other solutions. Those guesses reasonably near to the final structure or short-time solution all converged to the same solution while other initial guesses simply did not converge. The calculations were converged for all the systems studied for both sets of vertex functions. Following this, the rheological properties were determined by calculation of the Maxwell relaxation time for the shear viscosity, (64) or (70).

The results for the relaxation times are compared in Fig. 7. In each frame, experimental results for $\tau_2(k)$, $\tau_1(k)$, and $(1 - a(k))$ are shown from top to bottom as the points [note $(1 - a(k))$ being close to 1 means that $\tau_2(k)$ is more heavily weighted in the mean structural relaxation time]. The predictions for the two-body vertex functions are given as dashed lines while the convolution approximation is given as solid lines. The plots are given in experimental units of microseconds and inverse

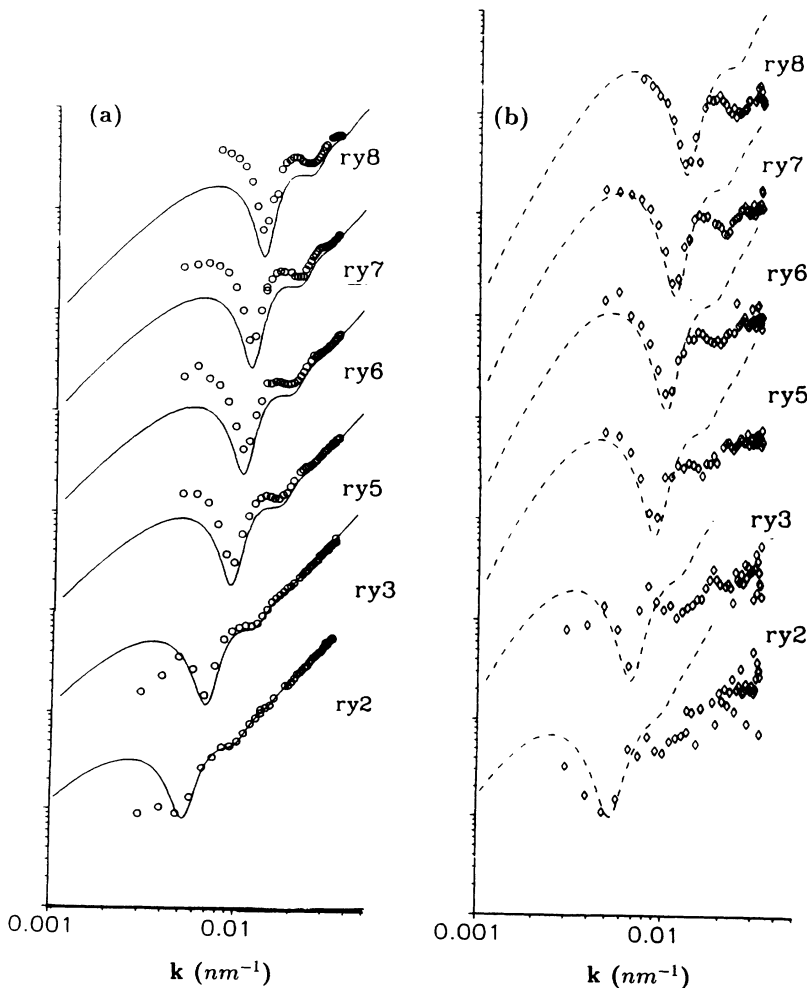


FIG. 6. (a) First cumulants, on a relative scale versus k (nm^{-1}), predictions (—) and experimental measurements (\circ). (b) Second cumulants, on a relative scale, versus k , (nm^{-1}), predictions (---) and experimental measurements (\diamond).

nanometers. The short-time approximation lies approximately midway between $\tau_2(k)$ and $\tau_1(k)$ for all systems and has the general shape of $\tau_2(k)$. The most significant component of the comparison is the peak in $\tau_2(k)$ and the value of $(1 - a(k))$ at the peak, which corresponds to the wave vector at the maximum in the equilibrium structure factor $S(k)$. Clearly, the two-body vertex function yields excellent predictions for $\tau_2(k)$ and $(1 - a(k))$, which are the dominant contribution to the mean structural relaxation time. This suggests that the coupling between suspension viscoelasticity and structural relaxation are correctly modeled through the mode-mode coupling. Clearly the convolution approximation overpredicts this coupling, which is not unexpected for superpositionlike approximations in general [14,24]. The two-body vertex function does underpredict the magnitude of $\tau_1(k)$, which is better represented by the convolution vertex function. The good agreement between theory and the published experiments demonstrates the power of keeping the self-consistency in solving the generalized hydrodynamics equations.

A comment must be made concerning the double-exponential nature of the dynamic structure factor. It is well known that many DLS experiments on charged systems can be simply approximated by such a double-exponential fit, but deviations are common [56]. This double-exponential fit is an approximate form of the full

generalized hydrodynamics theory that arises directly from the viscoelastic approximation. Thus deviations are to be expected in general. If the dynamic structure factor does exhibit reasonable double-exponential decay, then the viscoelastic approximation itself is expected to be satisfactory. Other workers using generalized hydrodynamics have advocated the use of spectrums, more exponentials [9], or Kohlrausch functions [16]. It would be reasonable then to make comparisons for cases where the double exponential form is not realized by comparing the mean structural relaxation time

$$\left[\begin{aligned} \tau_{S(k)}^m &= a(k)\tau_1(k) + (1 - a(k))\tau_2(k) \\ &= \frac{1}{S(k)} \int_0^\infty S(k, t) dt \end{aligned} \right]$$

for these cases. Clearly, for the above comparison with experiment the agreement with the mean structural relaxation time is almost perfect due to the good agreement of $\tau_2(k)$ and $(1 - a(k))$.

Figures 8(a) and 8(b) show typical examples for the dynamic viscosity functions, here for the two-body vertex functions, where the characteristic, viscoelastic behavior for a single Maxwell time is primarily observed. There is only a small deviation η'_s and η'_\parallel at high frequency due to $\tau_1(k)$ because it has little strength in the structure

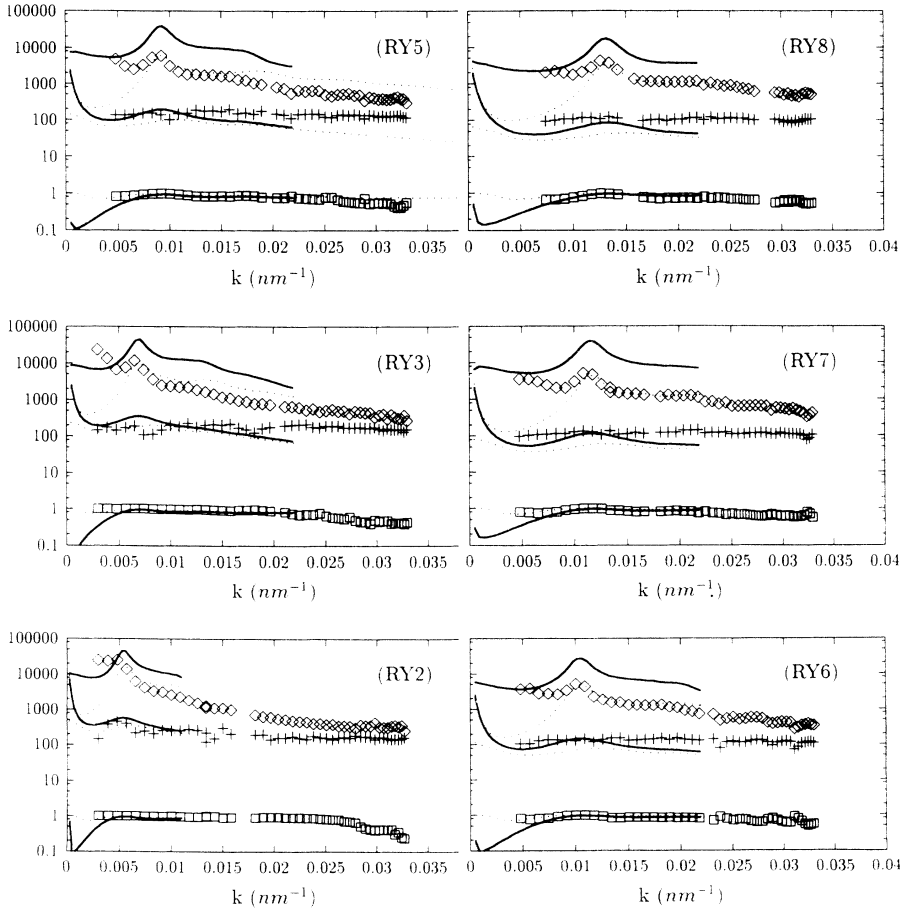


FIG. 7. τ_1 (+), τ_2 (\diamond), and $1 - a(k)$ (\square) as measured from DLS and predictions of theory, (---) two-body approximation, self-consistent solution, (- - -) convolution approximation, self-consistent solution. The units of the relaxation times are microseconds.

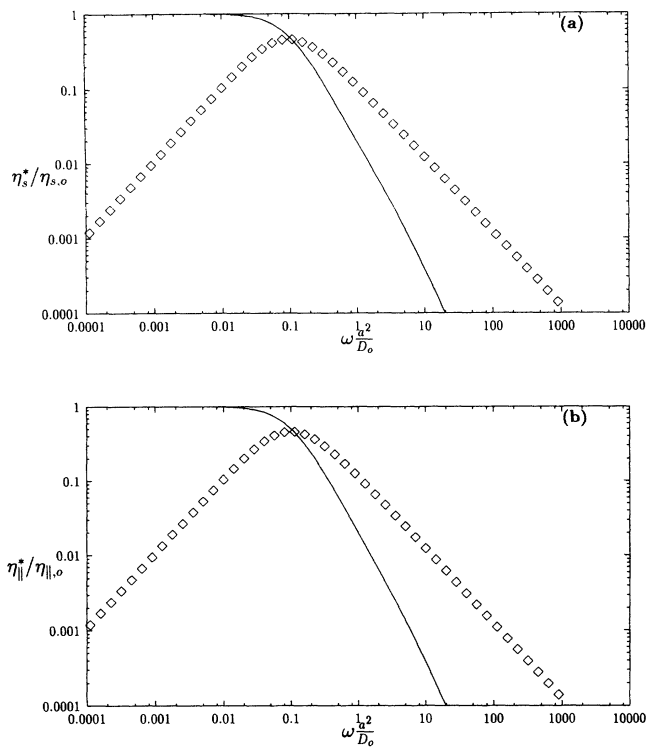


FIG. 8. (a) Normalized dynamic shear viscosity ($\eta_s^*/\eta_{s,o}$) for system RY5 versus dimensionless frequency $\omega \frac{a^2}{D_o}$, real part (—), complex part(\diamond). (b) Normalized dynamic longitudinal viscosity ($\eta_{\parallel}^*/\eta_{\parallel,o}$) for system RY5 versus dimensionless frequency $\omega \frac{a^2}{D_o}$, real part (—), complex part(\diamond).

relaxation. The results are qualitatively similar for the convolution approximation, just shifted to slightly lower frequency (longer time). For both vertex functions, coupling of suspension viscoelasticity to density fluctuations results in longer Maxwell relaxation times relative to the short-time solution. The relaxation times, for both vertex functions and for both short-time and VE approximations, are summarized in Figs. 9(a) and 9(b). The

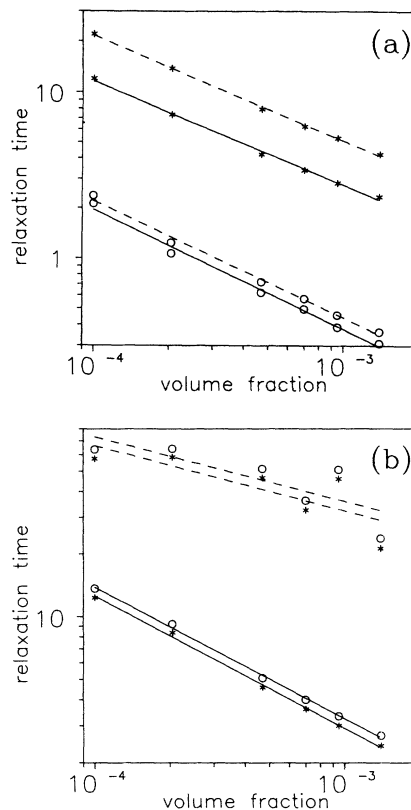


FIG. 9. (a) Predictions for the Maxwell relaxation times (dimensionless) for rheology for the DLS systems in the two-body approximation, short-time solution (—), self-consistent viscoelastic solution (- - -), τ_s^M (*), τ_{\parallel}^M (\circ). (b) Predictions for the Maxwell relaxation times for rheology for the DLS systems in the convolution approximation, same symbols as in A.

short-time solutions follow the Lindemann law Eq. (77), with the numerical coefficient increasing as one goes from short-time to full viscoelastic solution and in going from two-body to convolution approximation (see Table IV).

Important qualitative differences can be observed in comparing the two approximations for the vertex func-

TABLE IV. Rheological and dynamic power-law-fit parameters (property = $A\phi^\gamma$).

Property	Short-time		Viscoelastic	
	A	γ	A	γ
Two-body-vertex approximation				
τ_s^M	0.036	-0.63	0.067	-0.63
τ_{\parallel}^M	0.0027	-0.72	0.0035	-0.70
η_s	2.6	0.66	4.7	0.66
η_{\parallel}	3.3	0.29	4.3	0.27
$\Psi_{1,0}$	0.14	0.046	0.45	0.040
Convolution-vertex approximation				
τ_s^M	0.037	-0.63	0.042	-0.63
τ_{\parallel}^M	3.6	-0.32	4.2	-0.31
η_s	2.6	0.66	260.	0.97
η_{\parallel}	52.	0.34	5200	0.66
$\Psi_{1,0}$	0.15	0.039	1600	0.67

tions. As noted in the short-time analysis above, the two-body vertex function yields Maxwell times for longitudinal viscosity shorter than those for shear. Because the high frequency longitudinal elasticity is much larger than the shear modulus, the longitudinal viscosities remain larger than the shear viscosities. Thus there is a trend in going from weakly to strongly interacting systems suggesting that the longitudinal viscosity will eventually become less than the shear viscosity for the two-body approximation. The convolution approximation, however, yields distinctly different results for the Maxwell relaxation times such that the longitudinal Maxwell time is always longer than that corresponding to shear.

The rest of the rheological functions, as determined from the structural relaxation times, are summarized in Figs. 10(a) and 10(b). The two-body vertex functions result in viscosities that increase sublinearly with volume fraction and a normal stress coefficient $\Psi_{1,0}$ that is almost independent of volume fraction. When converted to real units it is clear that these mechanical properties cannot be measured to any accuracy using standard rheological equipment; so, no direct comparison with experiment is possible for these dilute systems. The coupling of density fluctuations to elasticity leads to an increase in the

rheological properties in all cases. For the convolution approximation, the increase in rheological properties in going from the short-time to the full viscoelastic solution is much more than for the two-body vertex, reflecting a stronger coupling between the longitudinal density fluctuations and the elasticity of the suspension. The primary normal stress coefficient $\Psi_{1,0}$ is found to be practically independent of volume fraction for both vertex approximations. The elongational pseudoviscosity, as calculated from Eq. (A6), leads to a Trouton ratio between 2.9 and 3.0 for all the systems studied. This is primarily a consequence of the large difference between the elastic and shear moduli (see Fig. 5). Table IV summarizes the power law fits to these rheological functions.

Also notice that the power-law exponents for the viscosity increase with volume fraction between two-thirds and one. This is just the contribution of the interparticle forces to the overall viscosity, so one would add the solvent plus the linear Einstein coefficient to get the measured viscosity. This result suggests that capillary viscometry measurements of these dilute, but strongly interacting, suspensions would give near linear plots with volume fraction. However, instead of measuring the intrinsic viscosity, the capillary viscometry will be strongly influenced by the interparticle forces. This phenomena has been recently reported for similar suspensions [69], and will be the subject of a future article [54].

2. Concentrated suspensions

The highly concentrated suspensions (see Table III) were prepared using the same batch of colloids by dialysis against a known salt solution of 1:1 electrolyte [67]. These suspensions vary in viscosity from waterlike to glassy, highly viscoelastic pastes, making it possible to accurately determine the low-shear limiting rheological response but unfeasible to measure the intermediate scattering function via DLS. In the experimental paper [50], the SANS data for the concentrated samples was fit by a five-component HNC-OZ polydisperse model. Due to the computational requirements of solving the five component problem, no RY-OZ solutions were performed. However, it was determined that the effective colloidal charge remained unchanged, along with, of course, the size and polydispersity. Direct comparison of theory and experiment for these limited systems can be made and the results are qualitatively and quantitatively similar to what follows. However, for clarity of understanding and to make a more meaningful and definitive comparison of the theoretical predictions with actual rheological measurements, an effective monodisperse fluid will be defined of the same number average size and charge with a Debye length given by the salt concentration of the dialysis bath. This enables us to explore the trends in the predictions and to compare with experiments over a much wider range of parameter space without introducing any additional complications or parameters. This mapping for the structure, as shown previously [59] and reproduced below, gives excellent results for direct comparison with wave-rigidity measurements of the high-frequency shear

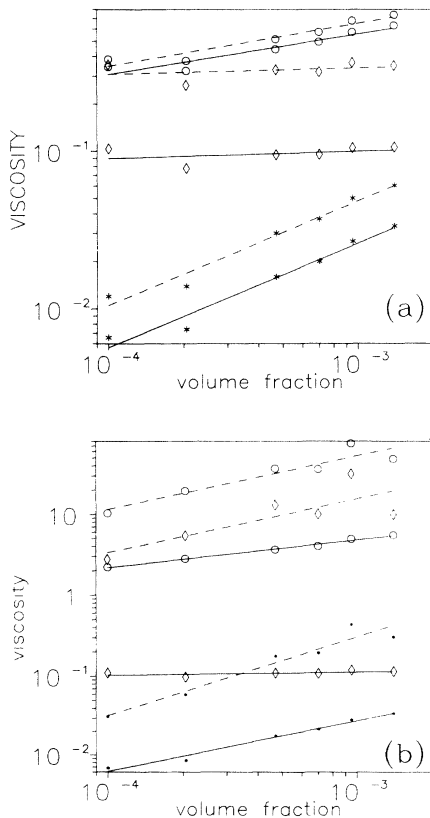


FIG. 10. (a) Predictions for the rheology (made dimensionless with the solvent viscosity) of the DLS systems in the two-body approximation, short-time solution (—), self-consistent viscoelastic solution (---), η_s (*), $\eta_{||}$ (○), Φ_1 (◇). (b) Predictions for the rheology of the DLS systems in the convolution approximation, short-time solution (—), self-consistent viscoelastic solution (---), η_s (*), $\eta_{||}$ (○), Φ_1 (◇).

elasticity, a property solely of the static structure and the intercolloidal potential.

The structure factors are shown in Figs. 11(a) and 11(b) for various volume fractions for the two series of 0.1 mM salt and 1.0 mM salt concentrations, respectively, corresponding to the first two system series in Table III. Using the rule that the peak in $S(k)$ exceeding 2.85 is indicative of a phase transition to the crystalline phase [68], it is apparent that structures from the dilute fluid into the metastable fluid regime are being investigated for both series. The thermodynamic properties of energy, pressure, and compressibility, as calculated from these structures, are shown for both systems in Figs. 12(a) and 12(b). They increase smoothly into the metastable fluid regime with the higher concentration showing an almost exponential rise.

Figure 13 shows the calculations for the high frequency shear modulus using this pseudomonodisperse fluid (hydrodynamic interactions are neglected, see [59]). As shown, the agreement is excellent in the qualitative behavior and for the quantitative overlap. Again, there are no adjustments in this calculation as both the microstructure and colloidal interaction potential are known. This result helps to justify the model as an accurate representation of the suspension. The predicted high-frequency shear elasticities also increase rapidly in the metastable fluid regime and are clearly well within the measured values. Thus the colloidal potential parameters used to fit

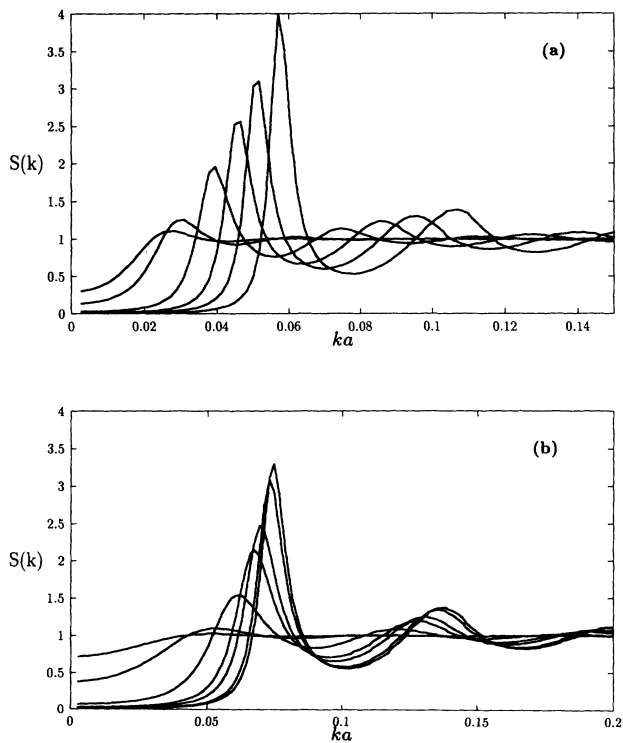


FIG. 11. (a) Thermodynamic structure factors for salt concentration 0.1 millimolar, volume fractions 0.005, 0.01, 0.03, 0.05, 0.07, and 0.1 with increasing peak height. (b) Thermodynamic structure factors for salt concentration 1 millimolar, volume fractions 0.01, 0.03, 0.10, 0.15, 0.17, 0.20, and 0.21 with increasing peak height.

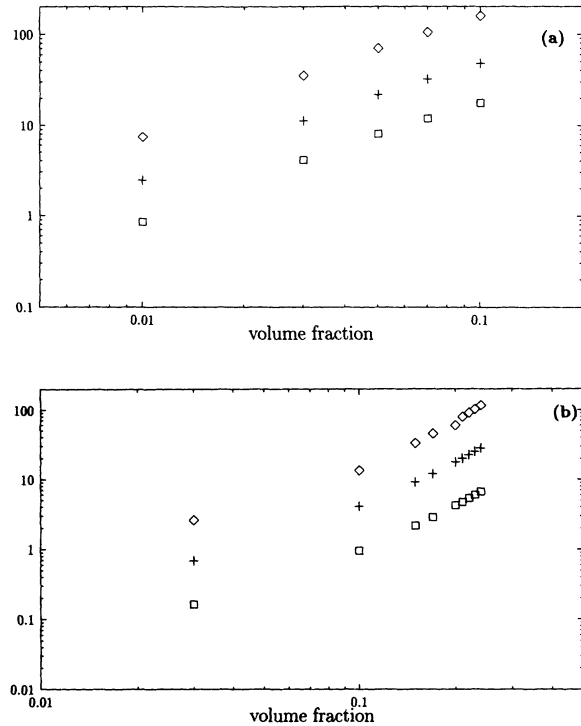


FIG. 12. Dimensionless compressibility (\diamond), pressure ($+$), and energy (\square) for systems at (a) 0.1 millimolar salt concentration, (b) 1 millimolar salt concentration.

the structure can also be used to predict high-frequency elasticities. This is especially encouraging as the elasticity is sensitive to the second derivative of the potential while the structure is sensitive to the magnitude of the potential and its derivative.

Using the same numerical scheme results in predictions for the dynamics, typified by the results presented in Figs. 14(a) and 14(b). The results for the two relaxation times and the weighting function in the viscoelastic approximation for the two-body vertex functions [14(a)] resemble those seen for the more dilute case (see Fig. 7). Also shown are the short-time solution and the Maxwell

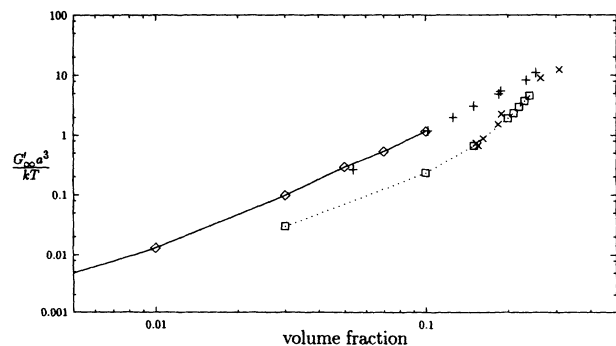


FIG. 13. High-frequency shear elasticity for systems at 0.1 millimolar salt concentration: measured ($+$), predicted ($-\diamond-$); and at 1 millimolar salt concentration: measured (\times), predicted ($-\square-$).

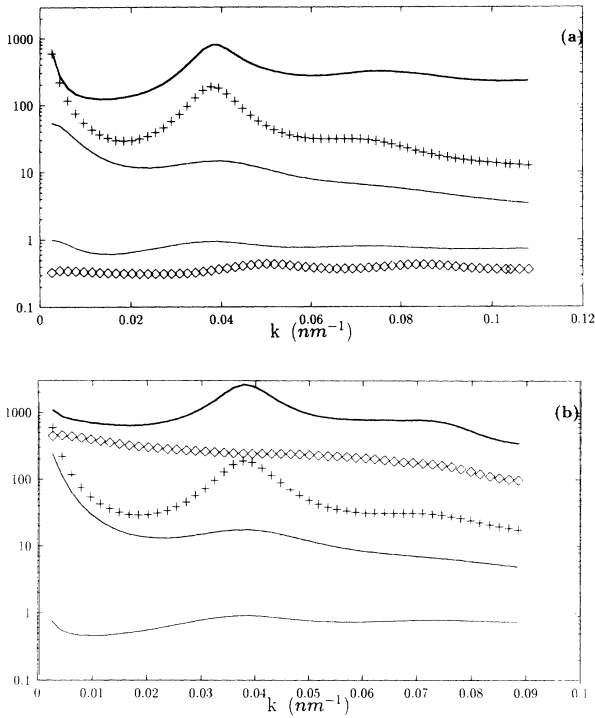


FIG. 14. Maxwell relaxation times for $\phi = 0.1$, $C^{\text{salt}} = 0.1$ millimolar. (a) two-body approximation, (b) convolution approximation. Symbols: τ_2 thick line, τ_1 medium line, $1 - a(k)$, thin line, τ_{\parallel}^M (\diamond), τ^{ST} (+).

relaxation time for the longitudinal viscosity, which is significantly lower than any of the other relaxation times. Notice how the dominant relaxation time τ_2 blends into the short-time solution at low wave vector, while τ_{\parallel}^M is significantly lower and τ_1 remains finite. This indicates that the strong-coupling limit has not been reached for this system and that coupling of density fluctuations to the suspension viscoelasticity remain weak. Such behavior is seen for both salt concentrations and all volume fractions examined.

The convolution approximation results in qualitatively different results for the same system. As seen in Fig. 14(b), τ_{\parallel}^M is now significantly larger than all but τ_2 . Notice that all of the relaxation times are shifted to higher values relative to the two-body approximation. The low-wave-vector behavior is now consistent with the strong-coupling limit outlined previously. That is, $\tau_2 \rightarrow \tau_{\parallel}^M$ which remains finite, but $\tau_1 \rightarrow \tau^{\text{ST}}$, which diverges. This transition to strong-coupling behavior increases as one increases the concentration. It is more apparent for the higher concentration system (1 mM salt), and results in a loss of solution. That is, for the higher concentrations of both series, this rapid increase of the τ_{\parallel}^M leads to a loss of convergence of the iterative solution technique employed here. No amount of regularization or change of parameters resulted in a stable, converged solution.

Predictions for the Maxwell relation times for shear and longitudinal viscosity are plotted in Figs. 15(a)–15(d). Again, the two closures give both quantitative and

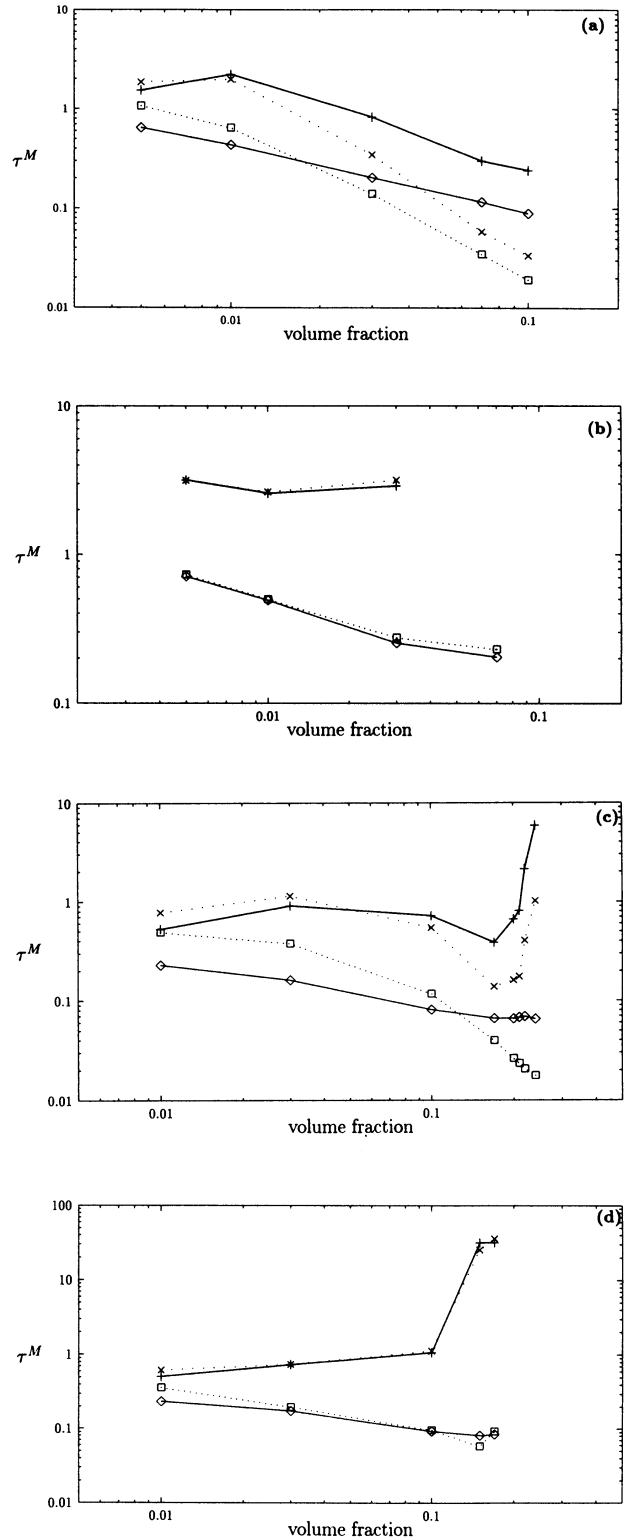


FIG. 15. Maxwell relation times for (a) 1 millimolar salt using the two-body vertex functions, (b) 1 millimolar salt using the convolution vertex functions, (c) 0.1 millimolar salt using the two-body vertex functions, (d) 0.1 millimolar salt using the convolution approximation. Symbols: τ_s^M for short-time approximation ($-\diamond-$), $\tau_{\parallel}^{\text{ST}}$ for short-time approximation ($-\square-$), τ_s^M for the viscoelastic calculation ($-+-$), τ_{\parallel}^M for the viscoelastic calculation ($-X-$).

qualitative differences. The two-body closure [15(a) and 15(c)] results in similar behavior as at the lower densities, where the longitudinal Maxwell times decrease faster than the shear with increasing concentration. The relaxation times predicted from the self-consistent viscoelastic approximation are significantly longer than those predicted for the short-time solution. The strong upturn for the 1mM salt concentration seen in the viscoelastic solution is well into the metastable fluid regime, but is, nonetheless, suggestive that a glass transition is being approached.

The convolution approximation, Figs. 15(b) and 15(d), show qualitatively different behavior and quantitatively longer relaxation times. As mentioned, convergent solutions were found only for the lower particle concentrations at both salt concentrations. For these predictions, the longitudinal relaxation time remains slightly larger than the shear, insuring that the viscosities will have

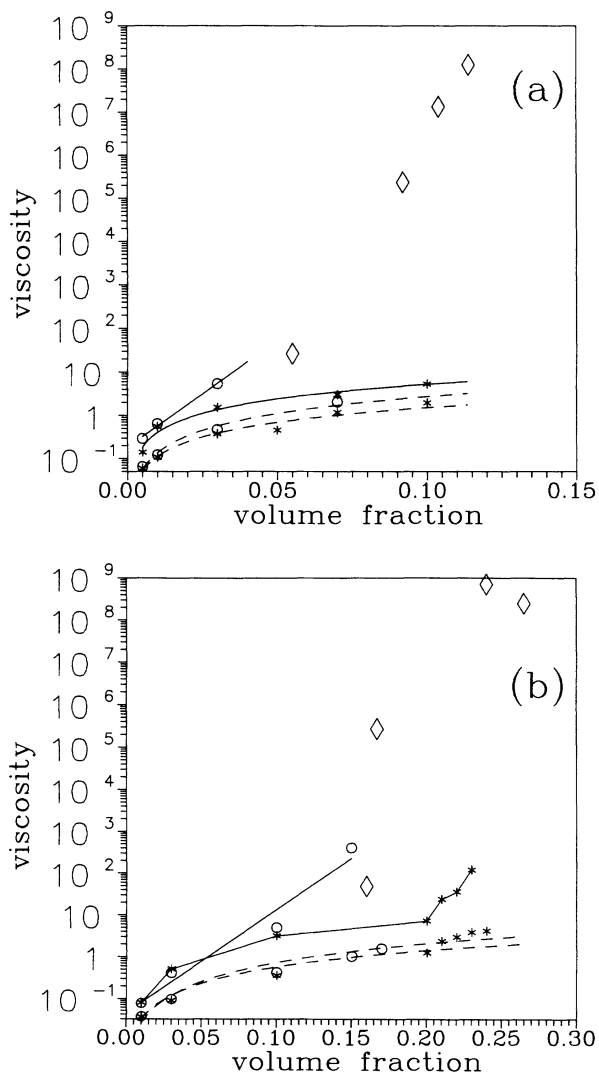


FIG. 16. Reduced interparticle viscosity (η/μ_0) for (a) 0.1 millimolar salt concentration and (b) 1.0 millimolar salt concentration. Symbols: measured (\diamond), viscoelastic (—), short time (---), convolution approximation (\circ), two-body approximation (*).

the same behavior. The strong coupling of density relaxations with suspension viscoelasticity result in longer longitudinal and shear relaxation times. The strong upturn and loss of solution for the 1mM viscoelastic solution was found to lead to an ideal-glass transition [70] using the technique of Bengtzelius *et al.* [71].

The rheological predictions from these models can now be directly compared against actual mechanical measurements of the shear viscosity, as shown in Figs. 16(a) and 16(b). As seen, the measurements of Goodwin *et al.* [67] show a strong increase in the low-shear limiting viscosity with added particle concentration. Clearly, the convolution approximation is able to qualitatively capture the exponential increase with volume fraction and is even quantitatively reasonable over the limited range of comparison. Notice how the actual viscosity diverges in the same region as the glass transition as predicted from the convolution approximation. All other predictions are both qualitatively and quantitatively in disagreement with the data. It is also to be noted that the pseudo-Trouton ratio is between two and three for all the predictions of the convolution approximation. The two-body approximation yields both negative and very large values as the longitudinal viscosity drops well below the shear viscosity. Furthermore, the predicted primary normal stress coefficients track the viscosity predictions but are still below normally accessible values.

3. Physical interpretation in terms of cage-melting

A popular method of envisioning the dynamics in simple and colloidal fluids is the cage-melting model [56]. In this model, the particles are temporarily localized, or “trapped” in a cage of their nearest neighbors. Diffusion for short times is confined to the cage, while for longer times, the cage “melts” and particles diffuse distances beyond the nearest neighbors. Colloidal transport is achieved by this process of cage melting, freeing the test particle to diffuse until the next cage is encountered. The general expression for the interparticle viscosity, $\eta_s = G'_\infty \tau_s^M$ is to be interpreted as G'_∞ representing the strength of the force localizing the particle in the cage (relative to shear deformations) and τ_s^M representing the melting time of the cage. The latter is modeled through extension of the Lindemann melting criterion for suspensions (see also [72]). This interpretation of the Lindemann law works as long as the melting time is simply controlled by free diffusion [20], as would be the case for the isolated cage. As has been shown here, this result is also recovered from the short-time approximation, which neglects coupling of density fluctuations to the suspension viscoelasticity.

The mode-mode-coupling solution can be interpreted as the consideration of the caging of these neighboring particles within a cage of their nearest neighbors, a “multiple cage” phenomena. Thus, for the nearest neighbor to diffuse so as to free the test particle, they themselves must escape their cages of nearest neighbors, and so on. Put another way, correlated motion of a collection of particles is required to dissipate the cage surrounding the

test particle. This intuitive picture helps to put in perspective the dependence of the transport coefficient upon collective dynamics of density fluctuations.

V. SUMMARY AND CONCLUSIONS

A method to calculate all of the collective dynamics and linear viscoelastic rheology for Brownian colloidal suspensions simply in terms of the fundamental physicochemical properties has been demonstrated. A self-consistent solution of the generalized hydrodynamics equations has been obtained numerically through the viscoelastic approximation. In this derivation, a further approximation must be made for the many-body correlations inherent in the mode-mode-coupling formalism. Two treatments for the mode-mode-coupling that are resident in the literature are rederived here and explained in terms of approximations for a three-body density correlation function.

The predicted structures and DLS and SANS measurements agree for these charged colloids interacting via a Yukawa potential. It is shown how to explicitly account for polydispersity effects for the structure, cumulants, and elastic constants. The good agreement of the calculated first and second cumulants and the high frequency shear elasticity over four orders of particle concentration further demonstrates the ability to model these charged suspensions via a Yukawa potential and the Rogers-Young-Ornstein-Zernike equation.

Calculations are performed to demonstrate the viscoelastic predictions for weakly correlated suspensions. Good agreement with the Lindemann melting rule and previous calculations based on a nonequilibrium Smoluchowski analysis were demonstrated. The relationship of these nonlinear equations for the transport properties and the Maxwell relaxation spectrum are also demonstrated.

Predictions for strongly correlated but dilute, in the volume fraction sense, suspensions of charged particles demonstrated the accuracy of the two-body approximation of Hess and Klein in modeling the dynamics. A large increase in the relaxation time above the Lindemann hypothesis is observed. The convolution approximation overestimates the three-body couplings and, hence, the coupling of density relaxations to the suspension viscosity.

Calculations for higher suspension concentrations, where added salt is needed to screen the electrostatic interactions, show the inadequacy of the two-body approximation to model the divergence of the relaxation time. The longitudinal relaxation time and viscosity decrease below that for the shear and no divergence in $\tau_{\parallel}^M(k)$ is observed. On the other hand, the convolution approximation, which has been used previously in studying the glass transition, demonstrates a strong divergence for the mechanical and collective properties.

Further work comparing this self-consistent solution against the details of Brownian dynamics simulations for model systems are currently under study to firm some of the interpretations and conclusions suggested by the

comparisons with actual measurements. This work complements current research using the generalized hydrodynamics formalism to describe both dilute suspensions and glass systems by providing a self-consistent solution valid for colloidal suspensions in the fluid phase. Future work includes the study of other Brownian systems relevant to the colloid community.

ACKNOWLEDGMENTS

This research was supported through the NSF (CTS 9158164) and NATO Collaborative Research Grant No. CRG 910465. Many helpful discussions with R. Klein and G. Nägele of Konstanz are gratefully acknowledged. The author is also indebted to Bruno D'Aguanno for help with the equilibrium structures and R. Krause, A.R. Rennie, S. Keeping, and Jim Goodwin for help with the quoted experimental data.

APPENDIX A: RHEOLOGICAL PROPERTIES STUDIED

Frequency dependent rheological measurements contain information about the dynamics of complex fluids. It is important to recognize that the results of the above-mentioned theories are limited to the linear response regime, and thus, the rheological characterization must be done in the linear viscoelastic limit. In a practical sense the deformation of the material during the measurement must be asymptotically small such that the response is linear. Within the context of the Onsager regression hypothesis and the fluctuation-dissipation theorem, the response of the suspension to its own internal fluctuations will be identical to the linear rheological response. Thus dynamical calculations of the stresses for an equilibrium suspension yields the linear transport coefficients of interest to the rheologist.

As a starting point we take the generalized Maxwell model for the relaxation spectrum of a complex fluid [73], consisting of an infinite superposition of Maxwell elements each with a characteristic relaxation time λ . The relaxation modulus is defined as

$$G(t) = \frac{\tau^{xy}(t)}{c_o^{xy}}. \quad (\text{A1})$$

where the experiment is a shear stress relaxation $\tau^{xy}(t)$ at infinitesimal shear strain levels c_o^{xy} .

The steady shear viscosity is defined as a time integral over the relaxation modulus

$$\eta_s = \int_0^\infty G(s) ds \quad (\text{A2})$$

and by frame invariance [74], the primary normal stress difference,

$$N_1 = \Psi_{1,0} \dot{\gamma}^2 = 2\dot{\gamma}^2 \int_0^\infty sG(s) ds. \quad (\text{A3})$$

Although not itself a linear property, the primary normal stress coefficient is related simply to the first term in an expansion for the shear modulus in frequency and, as such, can be obtained from the dynamic viscosity. Through linear viscoelasticity, the primary normal stress coefficient gives the recoverable strain upon flow cessation γ_∞^r as

$$\frac{\gamma_\infty^r}{\dot{\gamma}_0} = \frac{\frac{1}{2}\Psi_{1,0}}{\eta_s}, \quad (\text{A4})$$

showing this is zero in the limit of zero shear rate. The other relevant rheological function, the secondary normal stress coefficient, cannot be determined solely from linear viscoelasticity, as it depends on the choice of constitutive equation [74].

The steady elongational viscosity in the linear limit can also be expressed (for an incompressible fluid) as

$$\bar{\eta} = 3\eta_s, \quad (\text{A5})$$

leading to the Trouton ratio of 3. For a general, compressible fluid, this can be written as

$$\bar{\eta} = \frac{3\eta_s(\eta_{\parallel} - \frac{4}{3}\eta_s)}{\eta_{\parallel} - \eta_s}, \quad (\text{A6})$$

where η_{\parallel} is the longitudinal viscosity, which is calculated in a manner analogous to Eq. (A2) with $G_{\parallel}(t)$ replacing $G(t)$. In the model to be considered here, the OCF, the solvent is taken to be an incompressible, Newtonian fluid. The stresses from the solvent and the fluid of Brownian particles are taken to be additive. Thus, the elongational viscosity must be 3 as the longitudinal viscosity for the suspension as a whole is essentially infinite. However, it is still instructive to examine the contribution of the Brownian fluid to the longitudinal viscosity and the resultant elongational ‘‘pseudoviscosity’’ as the former property can be determined through optical techniques [75].

Defining the frequency-dependent modulus

$$G(\omega) = G'(\omega) + iG''(\omega), \quad (\text{A7})$$

yields

$$G'(\omega) = \omega \int_0^\infty G(t) \sin(\omega t) dt, \quad (\text{A8})$$

$$G''(\omega) = \omega \int_0^\infty G(t) \cos(\omega t) dt. \quad (\text{A9})$$

This function is also directly related to the frequency dependent shear viscosity:

$$\eta_s^*(\omega) = \eta_s'(\omega) - i\eta_s''(\omega) = \frac{G^*(\omega)}{i\omega}. \quad (\text{A10})$$

For such a general model this function may be written in terms of an infinite, linear superposition of relaxation times:

$$G(t) = \int_{-\infty}^\infty H(\lambda) e^{-t/\lambda} d \ln \lambda. \quad (\text{A11})$$

In the limits of a continuous distribution of relaxation times and linear response, this differential Maxwell model is equivalent to an integral model with the same relaxation spectrum $H(\lambda)$. Thus frequency-dependent moduli or viscosities can be written in terms of the relaxation time distribution function, again for a Maxwell model:

$$\eta_s'(\omega) = G''(\omega)/\omega = \int_0^\infty \frac{\omega\lambda}{1 + (\omega\lambda)^2} H(\lambda) d\lambda, \quad (\text{A12})$$

$$\eta_s''(\omega) = G'(\omega)/\omega = \int_0^\infty \frac{1}{1 + (\omega\lambda)^2} H(\lambda) d\lambda. \quad (\text{A13})$$

Consequently, either a stress relaxation at infinitesimal strain or a frequency-dependent viscosity-modulus measurement can be used to determine the relaxation spectrum, the low shear viscosity, and the high frequency limiting modulus. Further, the primary normal stress coefficient is related to the dynamic viscosity by

$$\Psi_{1,0} = \lim_{\omega \rightarrow 0} \frac{2\eta_s''}{\omega}. \quad (\text{A14})$$

Therefore, predictions of the time and wave vector dependent shear and longitudinal viscosity functions yields the full linear viscoelastic behavior for the suspension.

APPENDIX B: PRIMARY ELECTROVISCOUS EFFECT

The polarization of the Debye layer surrounding a colloid due to relative motion of the colloid, counterions, and solvent leads to a retardation force known as the primary electroviscous effect. This retardation manifests itself as an increase in the friction coefficient as measured through the first cumulant. There is a significant literature which treats aspects of this problem. Booth considered the electrolyte drag on the sedimentation velocity of a colloid by an asymptotic treatment of the entrainment of the

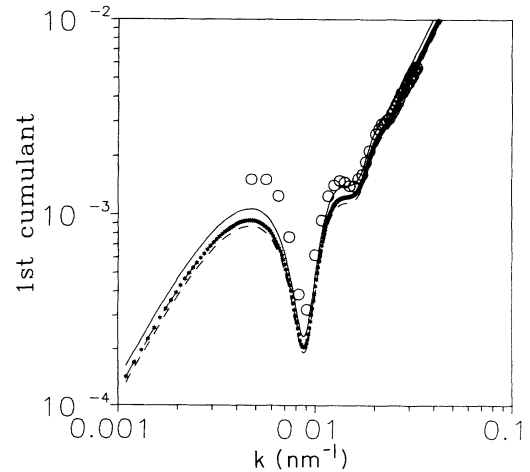


FIG. 17. System RY5, first cumulant: (O) DLS data, (—) without primary electroviscous effect correction, (---) Booth's correction, (- - -) Schurr's correction.

counterions in the Stokes flow field surrounding a moving macroion [76], but neglected any fluctuations in counterion concentration. Schurr [77] considers the effects of fluctuations in counterion concentration on the friction coefficient, neglecting hydrodynamic coupling. Comparison of these ideas have been discussed by Geigenmüller [78] and by Schurr [79]. Medina-Noyola and co-workers have examined the full dynamics of the fluctuations and their influence on the drag coefficient using a generalized Langevin equation approach [80–82]. It should be noted that the rheological and dynamical influences of the primary electroviscous effect have been treated at length by Russel [83], Dhont [32], and Felderhof and Jones [84]. However, for the strongly interacting systems considered in this paper, the secondary electroviscous effect is calculated to be many orders of magnitude more important for the viscosity than this primary effect.

When comparing explicit measurements of the first cu-

mulant with theory, however, this extra friction due to the Debye layer can be important. The two competing theories of Booth and Schurr were used to try and correct the first cumulant predictions for the DLS samples. For the relatively large Debye lengths of our systems ($\kappa a < 0.1$), the results of Schurr reduce to the classic Debye-Hückel results. Comparison of these two corrections for a typical sample are shown in Fig. 17. It is apparent that the added friction lowers the cumulant for both theories, but that the effect is minor. Comparison with the data shows better agreement at large scattering vector but worse agreement near the peak in $S(k)$. Although Schurr's correction is larger than that of Booth, the two theories are not distinguishable to within the accuracy of the data. Thus, as the peak in $S(k)$ plays a crucial role in the generalized hydrodynamics theory, the predicted first cumulant without any corrections for primary electroviscous effects is used throughout.

- [1] W. Hess and R. Klein, *Adv. Phys.* **33**, 173 (1983).
- [2] B.J. Ackerson, *J. Chem. Phys.* **64**, 242 (1976).
- [3] B.J. Ackerson, *J. Chem. Phys.* **69**, 684 (1978).
- [4] W. Hess, *Physica* **107A**, 190 (1981).
- [5] W. Hess, *J. Phys. A* **14**, L145 (1981).
- [6] R. Klein and W. Hess, *Faraday Discuss. Chem. Soc.* **76**, 137 (1983).
- [7] W. Hess and R. Klein, *Prog. Colloid Polym. Sci.* **69**, 174 (1984).
- [8] B. Cichocki and W. Hess, *Physica A* **141**, 475 (1987).
- [9] B. Cichocki and B.U. Felderhof, *J. Chem. Phys.* **96**, 9055 (1992).
- [10] R. Klein, in *Structure and Dynamics of Strongly Interacting Colloids and Supramolecular Aggregates in Solution*, edited by S.-H. Chen *et al.* (Kluwer Academic, Netherlands, 1992), p. 39.
- [11] *Statistical Mechanics: Part B: Time-Dependent Processes*, edited by B. J. Berne (Plenum, New York, 1977).
- [12] M.H. March and M.P. Tosi, *Atomic Dynamics in Liquids* (Dover, New York, 1976).
- [13] J.P. Boon and S. Yip, *Molecular Hydrodynamics* (McGraw-Hill, New York, 1980).
- [14] J.-P. Hansen and I.R. McDonald, *Theory of Simple Liquids* (Academic, London, 1986).
- [15] W. Götze, in *Liquids, Freezing and Glass Transition*, edited by J.-P. Hansen, D. Levesque, and J. Zinn-Justin (North-Holland, Amsterdam, 1989), pp. 288–503.
- [16] M. Fuchs, I. Hofacker, and A. Latz, *Phys. Rev. A* **45**, 898 (1992).
- [17] D.A. McQuarrie, *Statistical Mechanics* (Harper and Row, New York, 1976).
- [18] F.J. Rogers and D.A. Young, *Phys. Rev. A* **30**, 999 (1984).
- [19] B. D'Aguzzo, R. Klein, and N.J. Wagner, in *Complex Fluids*, MRS Symposia Proceedings No. 177 (Materials Research Society, Pittsburgh, 1990), p. 219.
- [20] H.M. Lindsay, W.D. Dozier, P.M. Chaiken, R. Klein, and W. Hess, *J. Phys. A* **19**, 2583 (1986).
- [21] G. Nägele, M. Medina-Noyola, R. Klein, and J.L. Arauz-Lara, *Physica A* **149**, 123 (1988).
- [22] R. Klein, W. Hess, and G. Nägele, *Physics of Complex and Supermolecular Fluids*, edited by S.A. Safran and N. A. Clark (Wiley, New York, 1987), p. 673.
- [23] J.-L. Barrat, W. Götze, and A. Latz, *J. Phys. Condens. Matter* **1**, 7163 (1989).
- [24] J.-L. Barrat, J.-P. Hansen, and G. Pastore, *Phys. Rev. Lett.* **58**, 2075 (1987).
- [25] I. Snook, W. van Meegen, and P. Pusey, *Phys. Rev. A* **43**, 6900 (1991).
- [26] H. Löwen, J.-P. Hansen, and J.-N. Roux, *Phys. Rev. A* **44**, 1169 (1991).
- [27] G.K. Batchelor and J.T. Green, *J. Fluid Mech.* **56**, 375 (1972); **56**, 401 (1972).
- [28] B.U. Felderhof, *Physica A* **147**, 203 (1987); **147**, 533 (1987).
- [29] W.B. Russel and A.P. Gast, *J. Chem. Phys.* **89**, 1580 (1988).
- [30] N.J. Wagner and W.B. Russel, *Physica A* **155**, 475 (1989).
- [31] N.J. Wagner and R. Klein, *Colloid Polym. Sci.* **269**, 295 (1991).
- [32] J.K.G. Dhont, *Physica A*, **146**, 541 (1987).
- [33] J.K.G. Dhont, *J. Fluid Mech.* **204**, 421 (1989).
- [34] D. Ronis, *Phys. Rev. A* **34**, 1472 (1986).
- [35] I.M. de Schepper, H.E. Smorenburg, and E.G.D. Cohen, *Phys. Rev. Lett.* **70**, 2178 (1993).
- [36] J.F. Brady, *J. Chem. Phys.* **99**, 567 (1993).
- [37] B.J. Ackerson and N.A. Clark, *Phys. Rev. A* **30**, 906 (1984).
- [38] B.J. Ackerson, J. van der Werff, and C.G. de Kruif, *Phys. Rev. A* **37**, 4819 (1988).
- [39] N.J. Wagner and W.B. Russel, *Phys. Fluids* **2**, 491 (1990).
- [40] S. Ashdown, I. Markovic, R.H. Ottewill, P. Lindner, R.C. Oberthur, and A.R. Rennie, *Langmuir* **6**, 303 (1990).
- [41] C.G. deKruif, W.J. Briels, R.P. May, and A. Vrij, *Langmuir* **4**, 668 (1988).
- [42] J.C. van der Werff, B.J. Ackerson, R.P. May, and C.G. de Kruif, *Physica A* **165**, 375 (1990).
- [43] S. Bell, G.M. Levine, and L.N. McCartney, *J. Colloid Interface Sci.* **33**, 335 (1970).
- [44] P. Hiemenz, *Principles of Colloid and Surface Chemistry*, 2nd ed. (Marcel Dekker, New York, 1986).
- [45] S. Alexander, D. Hone, P.M. Chaikin, P. Grant, and G.J.

- Morales, J. Chem. Phys. **80**, 5776 (1984).
- [46] H. Löwen and P.A. Madden, Phys. Rev. Lett. **68**, 1081 (1992).
- [47] H. Löwen, J.P. Hansen, and P.A. Madden, J. Chem. Phys. **98**, 3275 (1993).
- [48] W.B. Russel, D.A. Saville, and W. R. Schowalter, Colloidal Dispersions (Cambridge University Press, Cambridge, 1989).
- [49] B. D'Aguanno and R. Klein, J. Chem. Soc. Faraday Trans. **87**, 379 (1991).
- [50] N.J. Wagner, R. Krause, A.R. Rennie, B. D'Aguanno, and J. Goodwin, J. Chem. Phys. **95**, 494 (1991).
- [51] R. Krause, J.L. Aruaz-Lara, G. Nägle, H. Ruiz-Estrada, M. Medina-Noyola, R. Weber, and R. Klein, Physica A **178**, 241 (1991).
- [52] B. D'Aguanno, R. Klein, J.M. Méndez-Alcaraz, and G. Nägele (unpublished).
- [53] J.B. Hayter, in *Physics of Amphiphiles: Micelles, Vesicles and Microemulsions*: Proceedings of the International School of Physics, Enrico Fermi Course XC, Varenna, Italy, July, 1983, edited by V. Degiorgio and M. Corti (North-Holland, Amsterdam, 1985), p.59.
- [54] N.J. Wagner (unpublished).
- [55] J.C. Brown, P.N. Pusey, J.W. Goodwin, and R.H. Ottewill, J. Phys. A **8**, 664 (1975).
- [56] P.N. Pusey, J. Phys. A **11**, 119 (1978).
- [57] K.S. Schmitz, *Dynamic Light Scattering by Macromolecules* (Academic, Boston, 1990).
- [58] R. Zwanzig and R.D. Mountain, J. Chem. Phys. **43**, 4464 (1965).
- [59] N.J. Wagner, J. Colloid Interface Sci. **161**, 169 (1993).
- [60] T. Keyes, *Statistical Mechanics: Part B: Time-Dependent Processes*, edited by B.J. Berne (Plenum, New York, 1977), p. 259.
- [61] S. Hess, Phys. Rev. A **22**, 2844 (1980).
- [62] G. Szamel and H. Löwen, Phys. Rev. A **44**, 8215 (1991).
- [63] L. Sjörgen, Phys. Rev. A **22**, 2866 (1980).
- [64] H.J.M. Hanley, J.C. Rainwater, and S. Hess, Phys. Rev. A **36**, 1795 (1987).
- [65] U. Genz and R. Klein, Physica A **171**, 26 (1991).
- [66] C.J.W. Beenakker and P. Mazur, Phys. Lett. **98A**, 22 (1983).
- [67] S. Keeping, Ph.D. thesis, University of Bristol, 1989 (unpublished).
- [68] M.O. Robbins, K. Kremer, and G. Grest, J. Chem. Phys. **88** 3286 (1988).
- [69] F. Mallamace, F.N. Micali, and C. Vasi, Phys. Rev. A **42**, 7304 (1990).
- [70] N.J. Wagner (unpublished).
- [71] U. Bengtzelius, W. Götze, and A. Sjölander, J. Phys. C **17**, 5915 (1984).
- [72] H. Löwen, T. Palberg, and R. Simon, Phys. Rev. Lett. **70**, 1557 (1993).
- [73] W.R. Schowalter, *Mechanics of Non-Newtonian Fluids* (Pergamon, Oxford, 1978).
- [74] R. Larson, *Constitutive Equations for Polymer Melts and Solutions* (Butterworths, New York, 1988).
- [75] F. Grüner and W. Lehmann, J. Phys. A **12**, 303 (1979).
- [76] F. Booth, J. Chem. Phys. **22**, 1956 (1954).
- [77] J.M. Schurr, Chem. Phys. **45**, 119 (1980).
- [78] U. Geigenmueller, Chem. Phys. Lett. **110**, 666 (1984).
- [79] J.M. Schurr, Chem. Phys. Lett. **110**, 668 (1984).
- [80] M. Medina-Noyola and A. Vizcarra-Rendón, Phys. Rev. A, **32**, 3596 (1985).
- [81] H. Ruíz-Estrada, A. Vizcarra-Rendón, M. Medina-Noyola, and R. Klein, Phys. Rev. A **34**, 3446 (1986).
- [82] A. Vizcarra-Rendón, H. Ruíz-Estrada, M. Medina-Noyola, and R. Klein, J. Chem. Phys. **86**, 2976 (1987).
- [83] W.B. Russel, J. Fluid Mech. **85**, 209 (1978).
- [84] B.U. Felderhof and R.B. Jones, Faraday Discuss. Chem. Soc. **83**, 69 (1987).